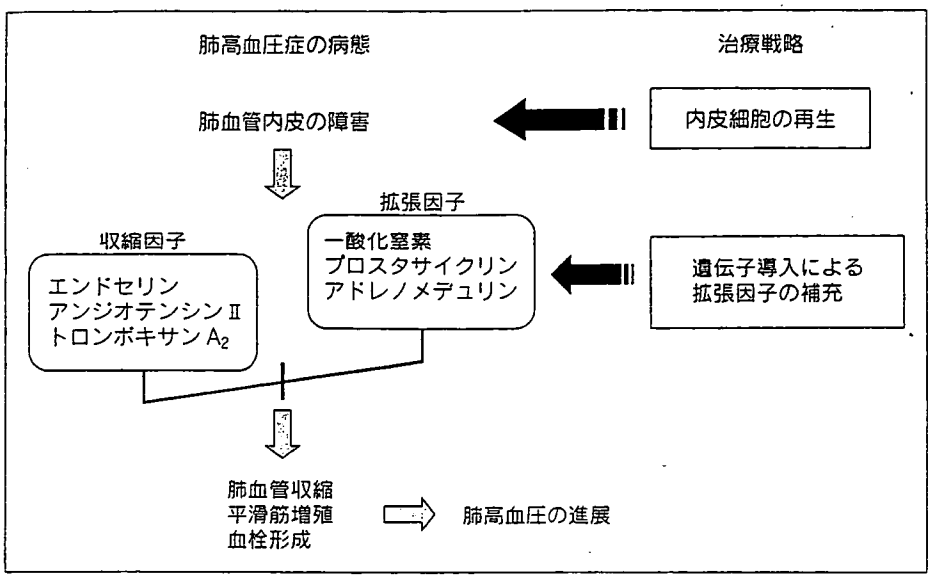

図3　肺高血圧症の病態に基づいた細胞-遺伝子ハイブリッド治療の戦略

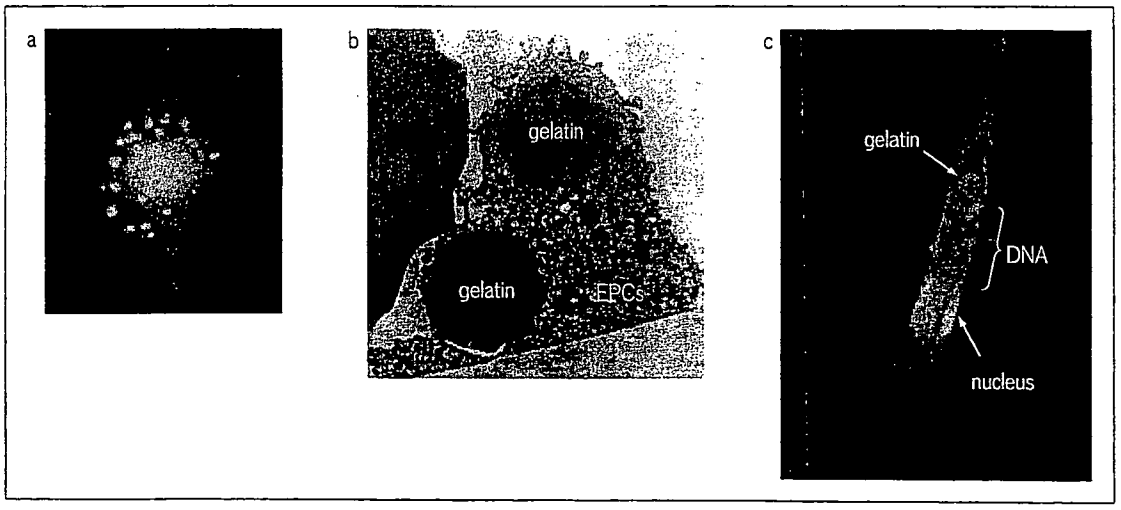

図4　ゼラチンを用いたEPCsへの遺伝子導入
a：ゼラチンに封入されたアドレノメデュリン遺伝（RITC-labeled）
b：ゼラチンを貪食した血管内皮前駆細胞
c：ゼラチンから細胞核に向かってDNAが放出される様子.

かになった.

モノクロタリン投与にて作製したラット肺高血圧モデルにアドレノメデュリン遺伝子を導入したEPCsを経静脈的に投与し，3週間後に肺高血圧の軽減効果を検討した[9]．EPCsは肺細動脈と間質に付着し，成熟した血管内皮細胞として血管を形成したが（図5a, b），EPCs単独投与では肺動脈の有意な低下には至らず，肺血管抵抗のわずか

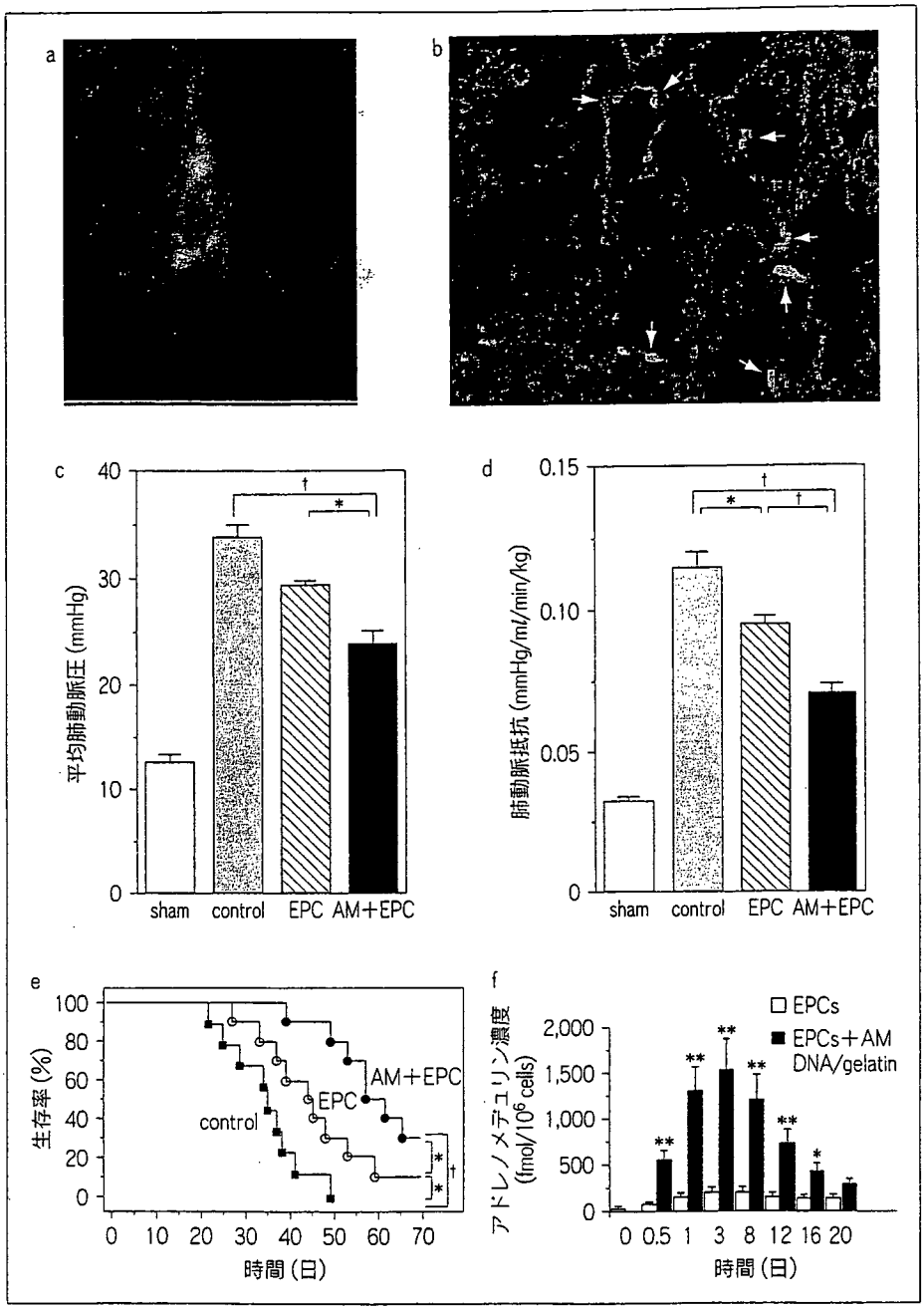

図 5　肺高血圧ラットに対する血管内皮前駆細胞とアドレノメデュリン遺伝子のハイブリッド治療の効果

a：GFP 遺伝子導入 EPCs.

b：GFP 発現 EPCs は，肺細動脈の内面や肺組織の間質に付着し，血管を形成した.

c, d, e：アドレノメデュリン遺伝子導入 EPCs の移植により，平均肺動脈圧，肺血管抵抗，および予後が有意に改善した. *：$p<0.05$, †：$p<0.01$

f：培養液中のアドレノメデュリン濃度. *：$p<0.05$, **：$p<0.01$ vs EPCs

な改善のみにとどまった．一方アドレノメデュリン遺伝子導入EPCsは平均肺動脈圧および平均肺動脈抵抗を有意に低下させ，生存率を有意に改善させた（図5c, d, e）．また，アドレノメデュリン遺伝子導入EPCsはEPCs単独の約10倍のアドレノメデュリンを分泌し，約3週間にわたって発現が持続した（図5f）．原発性肺高血圧症に対する治療としてプロスタサイクリン療法やエンドセリン受容体拮抗薬が開発され，その有効性が報告されているが，これらの治療にも抵抗性の症例が存在し，肺移植の適応とされながらもドナー不足により十分な治療が受けられないのが現状である．この細胞-遺伝子ハイブリッド治療が重症肺高血圧症に対する新たな治療法となる可能性がある．

おわりに

われわれが開発した生分解性ゼラチンを用いた遺伝子導入法は安全性，遺伝子の徐放化による持続発現の点で，従来のウイルスベクターを用いた方法よりも優れている可能性がある．本法は貪食能をもつ細胞であれば利用可能であると考えられ，肺高血圧症や虚血性心疾患などの難治性循環器疾患に対する新たな再生治療として期待されている．

文献

1) Isner JM, Pieczek A, Schainfeld R et al: Clinical evidence of angiogenesis after arterial gene transfer of phVEGF165 in patient with ischemic limb. Lancet 1996; **348**: 370–374
2) Tabata Y, Nagano A, Ikada Y et al: Biodegradation of hydrogel carrier incorporating fibroblast growth factor. Tissue Eng 1999; **5**: 127–138
3) Kasahara H, Tanaka E, Fukuyama N et al: Biodegradable gelatin hydrogel potentiates the angiogenic effect of fibroblast growth factor 4 plasmid in rabbit hindlimb ischemia. J Am Coll Cardiol 2003; **41**: 1056–1062
4) Kitamura K, Kangawa K, Kawamoto M et al: Adrenomedullin: a novel hypotensive peptide isolated from human pheochromocytoma. Biochem Biophys Res Commun 1993; **192**: 553–560
5) Tokunaga N, Nagaya N, Shirai N et al: Adrenomedullin gene transfer induces therapeutic angiogenesis in a rabbit model of chronic hind limb ischemia: benefits of a novel nonviral vector, gelatin. Circulation 2004; **109**: 526–531
6) Plautz G, Nabel EG, Nabel GJ et al: Introduction of vascular smooth muscle cells expressing recombinant genes *in vivo*. Circulation 1991; **83**: 578–583
7) Asahara T, Murohara T, Isner JM et al: Isolation of putative progenitor endothelial cells for angiogenesis. Science 1997; **275**: 964–967
8) Asahara T, Kawamoto A: Endothelial progenitor cells for postnatal vasculogenesis. Am J Physiol Cell Physiol 2004; **287**: C572–C579
9) Nagaya N, Kangawa K, Mori H et al: Hybrid cell-gene therapy for pulmonary hypertension based on phagocytosing action of endothelial progenitor cells. Circulation 2003; **108**: 889–895
10) Kawamoto A, Gwon HC, Iwaguro H et al: Therapeutic potential of *ex vivo* expanded endothelial progenitor cells for myocardial ischemia. Circulation 2001; **103**: 634–637
11) Tateishi-Yuyama E, Matsubara H, Murohara T et al: Therapeutic angiogenesis for patients with limb ischaemia by autologous transplantation of bone-marrow cells: a pilot study and a randomised controlled trial. Lancet 2002; **360**: 427–435
12) Nagaya N, Kyotani S, Uematsu M et al: Effects of adrenomedullin inhalation on hemodynamics and exercise capacity in patients with idiopathic pulmonary arterial hypertension. Circulation 2004; **109**: 351–356
13) Owji AA, Smith DM, Coppock HA: An abundant and specific binding site for the novel vasodilator adrenomedullin in the rat. Endocrinology 1995; **136**: 2127–2134
14) Nakamura M, Yoshida H, Makita S et al: Potent and long-lasting vasodilatory effects of adrenomedullin in humans. Comparisons between normal subjects and patients with chronic heart failure. Circulation 1997; **95**: 1214–1221

治療の歴史

血管新生療法

竹下　聡

はじめに

血管新生療法（therapeutic angiogenesis）[1]は，血管増殖因子やその遺伝子，あるいは骨髄や末梢血細胞を用いて血管新生を促進させ，組織虚血の改善を図る治療法である。循環器領域における初の遺伝子治療としても知られるvascular endothelial growth factor（VEGF）遺伝子を用いた血管新生療法が，米国のIsnerらによって行われたのは1994年のことである[2]。現在までにすでに10年以上が経過し，遺伝子以外にも増殖因子蛋白，骨髄細胞，末梢血細胞などを用いたさまざまな治療が試みられ，その有効性も検証されつつある。各々の治療法の詳細は他稿に譲り，ここでは血管新生療法がどのように生まれ，どのように育ってきたか，その歴史を概説する。

血管新生療法の臨床応用まで

血管新生療法のコンセプトそのものは決して新しいものではない。80年代後半には，ネコの虚血肢モデルに対して大網の脂質分画を投与し，虚血を改善させる試みが行われている。大網や脂肪細胞の再生医療への応用は最近のトピックであり，このような研究がすでに20年近く前に存在したことは興味に値する。これらの血管新生療法とIsnerらが行ったそれとの差異は，後者がVEGFという血管内皮細胞に特異的な増殖因子を用いた点にある。90年代初頭，Isnerらは家兎の虚血肢モデルにVEGF蛋白を投与し，血管新生療法の臨床応用を検討した。動脈投与，静脈投与，繰り返し投与，ヘパリンの併用などさまざまな投与法を検討し，投与法のいかんに関わらず，側副血行の促進には100～1000 μgのVEGF蛋白が必要なことを明らかにした。しかしながら，大量のVEGF蛋白を投与すると，投与した蛋白が全身を循環し，非目的部位へと到達するのは避け難い。血管増殖因子の全身への拡散は，糖尿病患者においては網膜症を悪化させ，癌患者では腫瘍血管の発達を促進させる。また，一部の血管増殖因子はNOを介した血管拡張作用を有し，遷延性低血圧を惹起する。事実，VEGF蛋白を用いた血管新生療法の臨床試験では，低血圧を避けるために投与量が制限された。

大量の蛋白投与に伴う副作用を回避するために行き着いた結論が遺伝子を用いたローカルドラッグデリバリーであった。Isnerらはカテーテルを用いて血管細胞へVEGF遺伝子を経皮的に導入し，それらの細胞からVEGF蛋白を分泌させようと考え，表面が親水性ゲルでコーティングされた冠動脈形成術用バルーンカテーテル（ハイドロゲル・バルーンカテーテル）による遺伝子導入を試みた。ハイドロゲルは，狭窄部位におけるバルーン通過性を改善するために施されたコーティングであるが，Isnerらはこのゲルにプラスミドの水溶液をしみ込ませ，遺伝子キャリアとして用いた。通常のPTCAテクニックによりバルーンを目的部位へと進め，4～8気圧で1分間バルーンを拡張させることで遺伝子の血管壁への導入が可能であった。その導入効率はリポゾームによる遺伝子導入に比し100倍以上の高効率ではあったが，βガラクトシダーゼ遺伝子を用いた組織的検討では，導入部位のわずか0.1%以下の細胞にしか遺伝子発現が認められなかった[3,4]。このわずかな細胞によって血管新生を促進することが可能なのかが問題となるのだが，遺伝子の導入効率（transfection efficiency）と治療効率（therapeutic efficiency）とは同義ではない。遺伝子産物である増殖因子が細胞外へと分泌されれば，たとえ導入効率は低くとも，パラクリン効果が期待できる[5]。この仮説は動物実験によって検証された。すなわち，ハイドロゲル・バルーンカテーテルを用いて家兎虚血肢モデルにVEGF遺伝子の導入を行うと，約3週間にわたりその発現が認められ，VEGF蛋白の動脈内投与と同等以上の側副路発達効果が得られたのである。一方，末梢血中のVEGF蛋白の濃度はELISAによる測定限界付近にあり，きわめて低値であった。つまり遺伝子の導入効率は低くとも，治療効果を得るに十分なVEGFの局所濃度が維持可能であり，逆に末梢血中濃度は希釈効果によって低く抑えられたのであ

たけした さとし：国立循環器病センター心臓血管内科

る。ここで忘れてならないのは，本法がプラスミドDNA以外には何らベクターを用いない遺伝子導入法（naked DNAアプローチ）である点で，臨床応用における高い安全性が期待された。

末梢動脈閉塞症に対するVEGFを用いた血管新生療法

1994年，Isnerらは血管新生療法の臨床試験を開始した[2]。この臨床試験は，循環器領域における初の遺伝子治療としても知られており，内科治療や外科治療不応性の重症末梢動脈閉塞症患者を対象として行われた。遺伝子治療から1〜2ヵ月で，血管造影上の新生血管出現が得られ，下肢疼痛や難治性潰瘍が消失した。副作用は下腿浮腫や良性血管腫など，一過性の軽微なものであった。しかしながら，バルーンカテーテルを用いた遺伝子導入は，動脈穿刺が不可能な例，下肢の動脈硬化が高度でカテーテルによるアプローチが困難な例，遺伝子導入に際し解離などの血管損傷リスクが高い例などには施行できない。そこで考案されたのが，虚血筋への遺伝子導入である[6]。Baumgartnerらは，VEGFプラスミドの筋注により，7〜8割の症例で血管造影上の側副路発達や臨床症状の改善を得ることに成功した[7]。この遺伝子導入法の単純化により，カテーテルでは治療困難であった症例にも血管新生療法が可能となり，その適応は大きく拡大することとなる。また，本法は心筋へも応用可能であり，虚血性心疾患に対する血管新生療法の臨床応用への契機となった。

虚血性心疾患に対するVEGFを用いた血管新生療法

90年代後半，Losordoらは胸部小切開法により重症狭心症患者の左室にVEGFプラスミドを筋注し，狭心症状の著明な改善と心筋シンチによる虚血所見の改善を得ることに成功した[8]。さらにLosordoらは，NOGAと呼ばれる心筋マッピングのシステムを用いて，心内膜側から経皮的にVEGF遺伝子の導入を行い，良好な治療効果を得た[9]。現在，このNOGAシステムを用いた経皮的遺伝子治療は，二重盲検試験によって検証中である。最近，類似のプロトコールを用いた臨床試験の結果がKastrupらにより報告されたが，VEGF治療群において左室壁運動の改善は認められたものの，自覚症状や心筋シンチ所見の改善は得られていない[10]。本法の有効性については，さらなる検討が必要である。

血管内皮前駆細胞の発見と細胞治療

遺伝子を用いた血管新生療法の臨床応用が進むなか，1997年，Asaharaらはヒト末梢血中のCD34陽性細胞の分画中に成熟内皮細胞へと分化しうる血管内皮前駆細胞（endothelial progenitor cell：EPC）が存在することを明らかにした[11]。これを契機として，遺伝子や蛋白を中心とした血管新生療法に，細胞移植を用いた血管新生療法の新しい流れが加わった。

EPCは血球血管芽細胞（ヘマンジオブラスト）と呼ばれる幹細胞より分化するが，成人では通常骨髄中にあり，末梢血中にはきわめてわずかしか存在しない。Kalkaらはヒト末梢血単核球からEPCを分離培養し，マウスの虚血肢モデルに投与することで下肢虚血の改善を得た[12]。一方，Shintaniらは自己骨髄由来単核球移植によって家兎虚血肢の血管新生が増強することを報告した[13]。移植された自己骨髄単核球が虚血組織における血管形成に参加，もしくは血管増殖因子を放出することで局所の血管新生を刺激したものと思われ，自己骨髄単核球細胞移植による血管新生療法の臨床応用への契機となった。

自己骨髄単核球細胞移植による血管新生療法

末梢動脈閉塞症に対する自己骨髄細胞移植の有用性は，2000年，国内3施設（久留米大学，関西医科大学，自治医科大学）によるTherapeutic Angiogenesis Using Cell Transplantation（TACT）trialにおいて示された[14]。全身麻酔下で採取した数百ccの骨髄液から単核球を分離後，虚血肢に移植することで，ABI（上肢・下肢血流比）は0.97ポイント増え，トレッドミル歩行距離は2.6倍に改善した。また，下肢疼痛は9割，皮膚潰瘍は8割の症例で改善した。同様のプロトコールを用いた多施設臨床試験がすでに実施されており，少なくとも本法の短期成績に関しては確立された治療法といっても過言ではない。

末梢血細胞を用いた血管新生療法の臨床応用に関しては，顆粒球コロニー刺激因子（granulocyte colony stimulating factor：G-CSF）を用いて末梢血中の単核球からCD34陽性細胞を分離したり，末梢血単核球細胞移植にアドレノメデュリンの局所投与を併用するなどさまざまな試みがなされている。その有効性に関してはまだ不明な点が多いものの，侵襲性の低さや細胞採取の容易さなど末梢血細胞移植の

メリットは大きく，今後の発展が期待される。

一方，虚血性心疾患に対する細胞治療に関しても，骨髄細胞の冠動脈内注入やNOGAシステムを用いた心筋内移植など，さまざまな臨床試験が進行中である。急性心筋梗塞患者の冠動脈内に骨髄単核球細胞を投与した初期の臨床試験では，梗塞サイズの減少や左室機能の改善，心筋バイアビリティーの改善が報告されているが，その治療効果については否定的な報告も少なくない。また，左室機能改善などの治療効果が血管新生によって得られたものなのか，あるいは心筋細胞の再生によるものなのか，その機序についても不明な点は多い。虚血下肢に対する細胞移植ほど確立された治療にはまだ至っていないというのが現状である。

おわりに

血管新生療法は血管増殖因子を用いた遺伝子治療として幕を開けた。しかしながら，遺伝子のパテント問題や倫理的ハードルの高さから，現在では細胞移植による血管新生療法が主流となりつつある。

虚血下肢に対する細胞移植の治療成績は良好であるが，臨床症状の改善にもかかわらず血管造影での改善を認めないことも少なくない。果たして細胞移植により血管新生が本当に促進されたのか？　単に潰瘍の創傷治癒機転が促進されただけではないのか？　その治療機序に関してはいまだ不明な点が少なくはなく，今後の研究成果が期待される。

文献

1) Takeshita S, Zheng LP, Brogi E, Kearney M, Pu LO, Bunting S, et al. J Clin Invest 1994；93：662-70.
2) Isner JM, Pieczek A, Schainfeld R, Blair R, Haley L, Asahara T, et al. Lancet 1996；348：370-4.
3) Takeshita S, Weir L, Chen D, Zheng LP, Riessen R, Bauters C, et al. Biochem Biophys Res Commun 1996；227：628-35.
4) Takeshita S, Tsurumi Y, Couffinahl T, Asahara T, Bauters C, Symes J, et al. Lab Invest 1996；75：487-501.
5) Takeshita S, Losordo DW, Kearney M, Rossow ST, Isner JM. Lab Invest 1994；71：387-91.
6) Tsurumi Y, Takeshita S, Chen D, Kearney M, Rossow ST, Passeri J, et al. Circulation 1996；94：3281-90.
7) Baumgartner I, Pieczek A, Manor O, Blair R, Kearney M, Walsh K, et al. Circulation 1998；97：1114-23.
8) Losordo DW, Vale PR, Symes JF, Dunnington CH, Esakof DD, Maysky M, et al. Circulation 1998；98：2800-4.
9) Vale PR, Losordo DW, Milliken CE, McDonald MC, Gravelin LM, Curry CM, et al. Circulation 2001；103：2138-43.
10) Kastrup J, Jorgensen E, Ruck A, Tagil K, Glogar D, Ruzyllo W, et al. J Am Coll Cardiol 2005；45：982-8.
11) Asahara T, Murohara T, Sullivan A, Silver M, van der Zee R, Li T, et al. Science 1997；275：964-7.
12) Kalka C, Masuda H, Takahashi T, Kalka-Moll WM, Silver M, Kearney M, et al. Proc Natl Acad Sci USA 2000；97：3423-7.
13) Shintani S. Circulation 2001；103：897-903.
14) Tateishi-Yuyama E, Matsubara H, Murohara T, Ikeda U, Shintani S, Masaki H, et al. Lancet 2002；360：427-35.

Acta Crystallographica Section F
Structural Biology and Crystallization Communications
ISSN 1744-3091

Tomoko Igarashi,[a] Yuko Oishi,[a] Satohiko Araki,[b] Hidezo Mori[a] and Soichi Takeda[a,c]*

[a]Department of Cardiac Physiology, National Cardiovascular Center Research Institute, 5-7-1 Fujishiro-dai, Suita, Osaka 565-8565, Japan, [b]Sugashima Marine Biological Laboratory, Graduate School of Science, Nagoya University, Toba, Mie 517-0004, Japan, and [c]Laboratory for Structural Biochemistry, Riken Harima Institute at SPring-8, 1-1-1 Kouto, Mikazuki, Sayo, Hyogo 679-5148, Japan

Correspondence e-mail: stakeda@ri.ncvc.go.jp

Received 11 May 2006
Accepted 12 June 2006

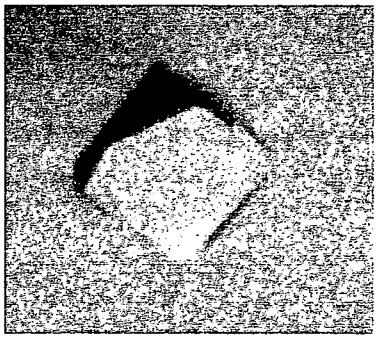

Crystallization and preliminary X-ray crystallographic analysis of two vascular apoptosis-inducing proteins (VAPs) from *Crotalus atrox* venom

VAPs are haemorrhagic snake-venom toxins belonging to the reprolysin family of zinc metalloproteinases. *In vitro*, VAPs induce apoptosis specifically in cultured vascular endothelial cells. VAPs have a modular structure that bears structural homology to mammalian ADAMs (a disintegrin and metalloproteinases). VAP1 is a homodimer with a MW of 110 kDa in which the monomers are connected by a single disulfide bridge. VAP2 is homologous to VAP1 and exists as a monomer with a MW of 55 kDa. In the current study, several crystal forms of VAP1 and VAP2 were obtained using the vapour-diffusion method and diffraction data sets were collected using SPring-8 beamlines. The best crystals of VAP1 and VAP2 generated data sets to 2.5 and 2.15 Å resolution, respectively.

1. Introduction

Haemorrhagic snake venoms contain factors that induce apoptosis specifically in cultured vascular endothelial cells (Araki *et al.*, 1993). The vascular apoptosis-inducing proteins VAP1 and VAP2 were originally isolated from the venom of the western diamondback rattlesnake *Crotalus atrox* (Masuda *et al.*, 1997, 1998) and similar apoptotic toxins (VAPs) have been isolated from other snake venoms (Masuda *et al.*, 2001; You *et al.*, 2003; Trummal *et al.*, 2005). VAP1 is a disulfide-bonded homodimeric protein with a molecular weight of 110 kDa and an isoelectric point of 8.5. VAP2 is an acidic single-chain protein with a molecular weight of 55 kDa and an isoelectric point of 4.5 (Masuda *et al.*, 1997, 1998). VAP1 (Masuda *et al.*, 2000) and VAP2 (S. Masuda, H. Hayashi & S. Araki, in preparation) are modular metalloproteinases with nucleotide-sequence homology to genes encoding the mammalian membrane-anchored metalloproteinases known as ADAMs. ADAMs are an emerging class of metalloproteinases whose function has been implicated in cell–cell and cell–matrix adhesion and signalling. They also appear to be associated with numerous diseases including arthritis, Alzheimer's disease and cancer (White, 2003; Blobel, 2005; Seals & Courtneidge, 2003; Moss & Bartsch, 2004; Duffy *et al.*, 2003).

Viperidae snake venoms contain a number of metalloproteinases, the snake-venom metalloproteinases (SVMPs), that induce local and systemic haemorrhage by disrupting the wall of the blood vessels in envenomed patients (Gutierrez *et al.*, 2005). All known VAPs belong to the P-III class of SVMPs, which have been shown to be the most potent haemorrhagic toxins from snake venoms. The P-III SVMPs have a modular structure consisting of metalloproteinase (M), disintegrin (D) and cysteine-rich (C) domains (Fox & Serrano, 2005). SVMPs and ADAMs are members of the reprolysin group of zinc-dependent metalloproteinases, which together with astasins, serralysin and matrix metalloproteinases comprise the metzincin superfamily of metalloproteinases (Bode *et al.*, 1993). All these enzymes share a signature consensus zinc-binding motif, HE*XX*H*XX*G*XX*H, in their catalytic region that defines proteins of the class, as well as a methionine-containing turn that serves as a structural base for the three active histidine residues (Bode *et al.*, 1993).

The crystal structures of several SVMPs of the P-I class, which contain only an M domain, and of isolated domains of ADAMs have

Table 1
Data-collection statistics for VAP1 crystals.

Values in parentheses are for the highest resolution shell. For each data set, a single crystal was used for measurement.

	Form 1-1	Form 1-2
Space group	$P4_12_12$	$P2_12_12_1$
Unit-cell parameters		
a (Å)	93.9	86.7
b (Å)	93.9	93.3
c (Å)	244.8	137.7
$\alpha = \beta = \gamma$ (°)	90	90
Beamline (detector)	BL45PX (Rigaku Jupiter)	BL45PX (Rigaku R-AXIS V)
Wavelength (Å)	0.98	1.0
Resolution (Å)	50–2.50 (2.59–2.50)	50–2.50 (2.59–2.50)
No. of unique reflections	38868 (3773)	38926 (3800)
R_{merge}†	0.084 (0.380)	0.072 (0.369)
$I/\sigma(I)$	18.7 (7.1)	14.4 (2.9)
Completeness (%)	99.7 (99.6)	99.4 (98.8)
Redundancy	12.7	3.91
No. of molecules in ASU	1	1
Matthews value (Å^3 Da^{-1})	2.5	2.5
Solvent content (%)	51	51

† $R_{merge} = \sum_{hkl}\sum_i |I_i(hkl) - \langle I(hkl)\rangle| / \sum_{hkl}\sum_i I_i(hkl)$, where $I_i(hkl)$ is the ith intensity measurement of reflection hkl and $\langle I(hkl)\rangle$ is its average.

been determined. However, structures of SVMPs or ADAMs containing M, D and C domains have not been determined. To understand more about the structure of P-III SVMPs and ADAMs and how it relates to the molecular mechanism of VAP-induced apoptosis, we initiated the crystallographic analysis of VAP1 and VAP2. This is the first report of the crystallization and preliminary X-ray analysis of apoptotic SVMPs. Three-dimensional crystal structures of VAP1 derived from the two distinct crystal forms described in this report have recently been described (Takeda *et al.*, 2006); the structural analysis of VAP2 is ongoing.

2. Methods

2.1. Purification

VAP1 and VAP2 were purified as described previously (Maruyama *et al.*, 2005; Masuda *et al.*, 1998) with some modifications. Briefly, crude *C. atrox* venom (Sigma–Aldrich, USA) was dissolved in buffer containing 10 m*M* Tris–HCl pH 7.0 and 10 m*M* NaCl and then applied onto a CM-Sepharose (Amersham Bioscience, USA) column equilibrated with the same buffer. VAP2 was eluted from the column with the above buffer, whereas VAP1 was eluted with buffer containing 10 m*M* Tris–HCl pH 7.0 and 50 m*M* NaCl.

The VAP1 was further purified on a hydroxylapatite column. The VAP1-containing CM-Sepharose fraction was first diluted with an equal amount of distilled water and then applied onto a hydroxylapatite column equilibrated with 25 m*M* sodium phosphate pH 7.0. VAP1 was eluted using buffer containing 50 m*M* sodium phosphate pH 7.0 and then concentrated using an Amicon Ultra membrane (Millipore) with a nominal molecular-weight limit (NMWL) of 50 000 Da. The final protein concentration was 6.5 mg ml^{-1}. During the concentration step, the buffer was replaced with 10 m*M* Tris–HCl pH 7.0.

The VAP2-containing CM-Sepharose fraction was loaded onto a Resource Q (GM Healthcare) column equilibrated with 10 m*M* Tris–HCl pH 8.0 and 50 m*M* NaCl and then eluted with a gradient of NaCl. 55 kDa molecular-weight fractions, which were eluted at about 130 m*M* NaCl, were pooled and concentrated by Amicon Ultra with a 30 000 NMWL membrane. The final protein concentration was 3.8 mg ml^{-1} in buffer containing 10 m*M* Tris–HCl pH 8.0.

2.2. Initial crystallization screen

Initial screening for appropriate crystallization conditions for VAP1 and VAP2 was carried out using the sitting-drop vapour-diffusion method and Crystal Screen (Hampton Research, USA), with or without 63 µg ml^{-1} (almost twice the molar protein concentration) of the hydroxyamate inhibitor 3-(*N*-hydroxycarboxamide)-2-isobutyl-propanoyl-Trp-methylamide (GM6001, Calbiochem) in the protein solution. A volume of 0.3–0.5 µl protein solution was mixed with an equal amount of reservoir solution and droplets were allowed to equilibrate against 0.1 ml reservoir solution at 293 K.

2.3. Diffraction data collection

Crystals were cryoprotected, mounted in a nylon loop (Hampton Research, USA) or in a Lytho Loop (Protein Wave Corp., Japan) and immediately exposed to a stream of nitrogen gas at 100 K to flash-freeze the samples. The preliminary X-ray data were collected using an in-house X-ray diffractometer (Rigaku Micromax-007 X-ray generator with R-AXIS VII imaging-plate detector) and crystals that diffracted well were selected for data acquisition using the beamlines at SPring-8. All diffraction data sets were collected using undulator beamlines (BL41XU, BL45XU) at 100 K and diffraction images were processed using the *HKL*2000 software (Otwinowski & Minor, 1997).

3. Results

3.1. VAP1 crystals

3.1.1. Crystallization. VAP1 was reproducibly crystallized in two distinct crystal forms. Crystals were initially obtained using Crystal

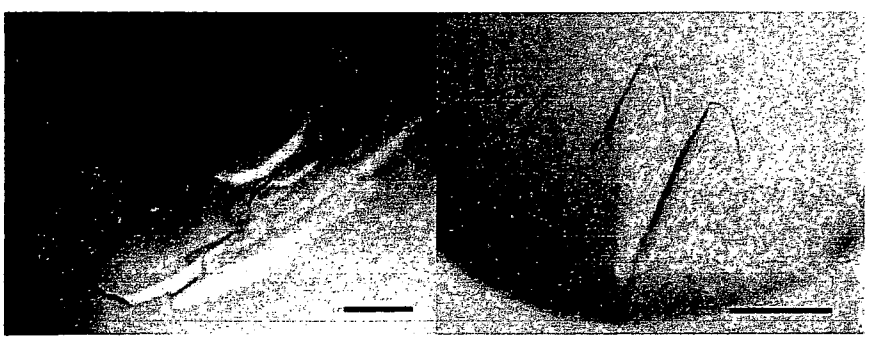

(*a*) (*b*)

Figure 1
VAP1 crystals. (*a*) Form 1-1. (*b*) Form 1-2. The scale bars indicate 0.1 mm.

Table 2
Data-collection statistics for VAP2 crystals.

Values in parentheses are for the highest resolution shell. For each data set, a single crystal was used for measurement.

	Form 2-1	Form 2-2	Form 2-3	Form 2-4	Form 2-5
GM6001	+	+	+	+	−
Space group	$P2_1$	$P2_12_12_1$	$P4_1$	$P6_322$	$C2$
Unit-cell parameters					
a (Å)	56.9	57.7	60.7	156.8	220.7
b (Å)	138.0	118.2	60.7	156.8	79.5
c (Å)	59.2	138.5	257.9	95.6	58.7
α (°)	90	90	90	90	90
β (°)	91.5	90	90	90	91.7
γ (°)	90	90	90	120	90
Beamline (detector)	BL41XU (ADSC Quantum 310R CCD detector)				
Wavelength (Å)	1.0	1.0	1.0	1.0	1.0
Resolution (Å)	50–2.15 (2.23–2.15)	50–2.50 (2.59–2.50)	50–3.20 (3.31–3.2)	50–3.80 (3.94–3.80)	50–2.70 (2.80–2.70)
No. of unique reflections	48664 (4428)	33288 (2925)	15097 (1437)	7169 (682)	26911 (2313)
R_{merge}†	0.081 (0.196)	0.089 (0.321)	0.091 (0.360)	0.117 (0.397)	0.085 (0.231)
$I/\sigma(I)$	9.8 (4.6)	10.3 (3.7)	10.9 (4.0)	8.4 (6.5)	10.1 (5.5)
Completeness (%)	98.1 (89.5)	98.6 (88.4)	99.5 (95.7)	99.8 (99.9)	95.9 (82.5)
Redundancy	3.3	6.5	7.0	19.2	3.4
No. of molecules in ASU	2	2	2	1	2
Matthews value (Å^3 Da^{-1})	2.4	2.4	2.5	3.1	2.7
Solvent content (%)	49	49	50	60	54

† $R_{merge} = \sum_{hkl}\sum_i |I_i(hkl) - \langle I(hkl)\rangle| / \sum_{hkl}\sum_i I_i(hkl)$, where $I_i(hkl)$ is the ith intensity measurement of reflection hkl and $\langle I(hkl)\rangle$ is its average.

Screen solution No. 46, but these crystals diffracted poorly. Subsequently, droplets were prepared by mixing 1 µl protein solution and 1 µl reservoir solution containing 15% PEG 8000, 0.1 *M* sodium cacodylate pH 6.5 and then equilibrated against 1 ml reservoir solution. Within a couple of weeks, using the hanging-drop method, improved tetragonal crystals (form 1-1; Fig. 1*a*) were obtained.

Orthorhombic crystals (form 1-2; Fig. 1*b*) were obtained using Additive Screen (Hampton Research, USA). The droplet was made by mixing 0.3 µl protein solution and 0.3 µl reservoir solution supplemented with one-fifth of the volume of 0.1 *M* cobalt(II) chloride (Additive Screen solution No. 4). The best crystals were obtained using the sitting-drop method after equilibration for 3 d against 0.1 ml of the same reservoir solution used to obtain form 1-1 crystals.

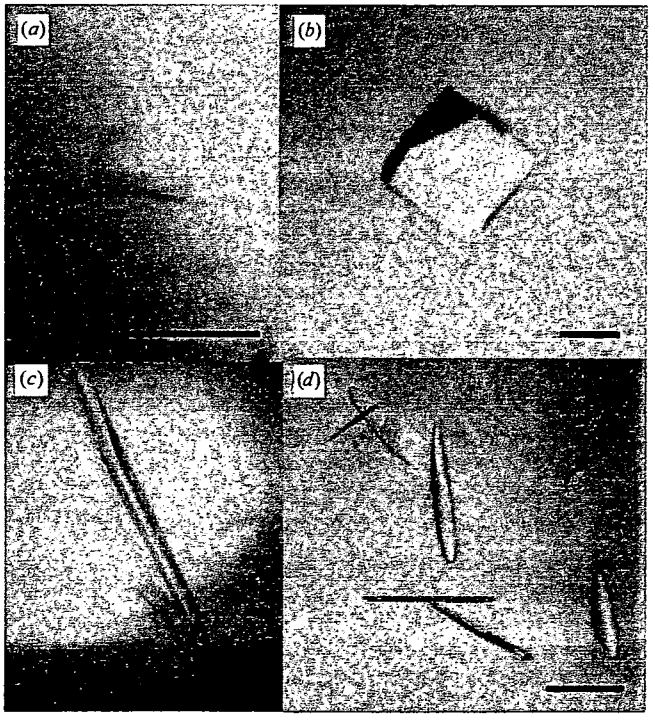

Figure 2
VAP2 crystals. (*a*) Form 2-2, (*b*) form 2-3, (*c*) form 2-4 and (*d*) form 2-5 crystals. The scale bars indicate 0.1 mm.

3.1.2. X-ray analysis. For X-ray measurements, crystals of either crystal form were soaked in a solution containing 15% PEG 8000, 5% methanol, 20% xylitol and 0.1 *M* sodium cacodylate pH 6.5 for cryoprotection prior to flash-freezing. X-ray diffraction data were obtained by the oscillation method using beamline BL45XU and an oscillation angle of 0.75° per image. Data sets were collected using a CCD detector (Rigaku Jupiter) for crystal form 1-1 or an imaging-plate detector (Rigaku R-AXIS V) for crystal form 1-2. The unit-cell parameters and the data statistics for the two crystal forms are summarized in Table 1. The structures were determined at 2.5 Å resolution by the molecular-replacement method using the P-I SVMP acutolysin-C (PDB code 1qua) as a starting model (Takeda *et al.*, 2006). The coordinates and the structure factors have been deposited in the PDB (2erq for form 1-1 and 2ero for form 1-2 crystals).

3.2. VAP2 crystals

3.2.1. Crystallization. Five distinct crystal forms of VAP2 were analyzed by X-ray diffraction. The initial screening for VAP2 crystals was performed in the presence and absence of the inhibitor GM6001.

In the presence of GM6001, Crystal Screen solution No. 10 yielded crystals. With this as a starting condition, the pH of the mother liquor, the PEG concentration and molecular weight and the species and concentrations of salts and additives were optimized and four distinct crystal forms were obtained (forms 2-1, 2-2, 2-3 and 2-4). These four forms were only obtained in the presence of GM6001 and were never obtained in its absence. Monoclinic (form 2-1) and orthorhombic (form 2-2; Fig. 2*a*) forms were obtained by the sitting-drop method under identical conditions as follows: droplets were made by mixing 0.5 µl protein solution with 0.5 µl reservoir solution containing 30% PEG 8000, 0.1 *M* ammonium acetate, 0.1 *M* sodium cacodylate pH 6.5 and were equilibrated against 0.1 ml reservoir solution. Tetragonal form crystals (form 2-3; Fig. 2*b*) were obtained by adding a one-tenth volume of 1 *M* potassium chloride (Additive Screen solution No. 16)

to the mother liquor and using a reservoir solution containing 30% PEG 8000, 0.1 *M* ammonium acetate, 0.1 *M* sodium acetate pH 4.6 with the same drop and reservoir volumes described above. Hexagonal crystals (form 2-4; Fig. 2*c*) were obtained by the hanging-drop method using 1 ml of a reservoir solution containing 20% PEG 20 000, 0.2 *M* calcium acetate, 0.1 *M* sodium cacodylate pH 6.5. The droplet was made by mixing 1 µl protein solution and 1 µl reservoir solution supplemented with a one-fifth volume of 0.3 *M* glycyl-glycyl-glycine solution (Additive Screen solution No. 34).

In the absence of GM6001, crystals were obtained with Crystal Screen solution No. 46, but these crystals yielded poor diffraction data. To improve the quality of the crystals, several additives were screened. Monoclinic crystals (form 2-5; Fig. 2*d*) were obtained by adding a one-tenth volume of 40% *n*-propanol solution (Additive Screen solution No. 90) to the reservoir solution (final composition 4% *n*-propanol, 16.2% PEG 8000, 0.18 *M* calcium acetate, 0.09 *M* sodium cacodylate pH 6.5). A mixture of 0.5 µl protein solution and 0.5 µl reservoir solution was equilibrated against 0.1 ml reservoir solution. These form 2-5 crystals were only obtained in the absence of GM6001 and were never obtained in its presence.

3.2.2. X-ray analysis. The mother liquors of the form 2-2 and 2-3 crystals were suitable for freezing; all others were first cryoprotected. For form 2-1 and 2-4 crystals, 20% glycerol was added to the reservoir solution for cryoprotection. For form 2-1, the cryogenic solution was added gradually to the crystal droplet in order to avoid cracking induced by osmotic shock. Crystal form 2-5 was rinsed in a solution containing 15% PEG 8000, 5% methanol, 20% xylitol and 0.1 *M* sodium cacodylate pH 6.5 and then immediately flash-frozen at 100 K. Because these crystals were extremely thin and fragile, they were mounted in a LithoLoop, an etched Mylar film, to prevent bending of the crystal.

All diffraction data sets for the VAP2 crystals were acquired using the oscillation method and beamline BL41XU (the oscillation angle was 1.0° for all data sets) at a wavelength of 1.0 Å and data were collected using an ADSC Quantum 310R detector. The unit-cell parameters and statistics for the data sets are summarized in Table 2. The estimated number of molecules in the asymmetric unit for each crystal form was obtained by a preliminary molecular-replacement method using *MOLREP* from the *CCP*4 suite (Collaborative Computational Project, Number 4, 1994) and the metalloproteinase (M) and cysteine-rich (C) domains of VAP1 (Takeda *et al.*, 2006) as the starting models. Structural analyses of these crystals along with the molecular-replacement phases are ongoing.

We thank Mariko Tomisako for her help in crystallization experiments and the staff of SPring-8 for assistance with data acquisition. This work was partly supported by Grant Nano-001 for Research on Advanced Medical Technology from the Ministry of Health, Labour and Welfare of Japan and by grants from the Takeda Science Foundation, from the Kao Foundation for Arts and Science and from the Senri Life Science Foundation.

References

Araki, S., Ishida, T., Yamamoto, T., Kaji, K. & Hayashi, H. (1993). *Biochem. Biophys. Res. Commun.* **190**, 148–153.
Blobel, C. P. (2005). *Nature Rev. Mol. Cell Biol.* **6**, 32–43.
Bode, W., Gomis-Ruth, F. X. & Stockler, W. (1993). *FEBS Lett.* **331**, 134–140.
Collaborative Computational Project, Number 4 (1994). *Acta Cryst.* D**50**, 760–763.
Duffy, M. J., Lynn, D. J., Lloyd, A. T. & O'Shea, C. M. (2003). *Thromb. Haemost.* **89**, 622–631.
Fox, J. W. & Serrano, S. M. (2005). *Toxicon*, **45**, 969–985.
Gutierrez, J. M., Rucavado, A., Escalante, T. & Diaz, C. (2005). *Toxicon*, **45**, 997–1011.
Maruyama, J., Hayashi, H., Miao, J., Sawada, H. & Araki, S. (2005). *Toxicon*, **46**, 1–6.
Masuda, S., Araki, S., Yamamoto, T., Kaji, K. & Hayashi, H. (1997). *Biochem. Biophys. Res. Commun.* **235**, 59–63.
Masuda, S., Hayashi, H. & Araki, S. (1998). *Eur. J. Biochem.* **253**, 36–41.
Masuda, S., Hayashi, H., Atoda, H., Morita, T. & Araki, S. (2001). *Eur. J. Biochem.* **268**, 3339–3345.
Masuda, S., Ohta, T., Kaji, K., Fox, J. W., Hayashi, H. & Araki, S. (2000). *Biochem. Biophys. Res. Commun.* **278**, 197–204.
Moss, M. L. & Bartsch, J. W. (2004). *Biochemistry*, **43**, 7227–7235.
Otwinowski, Z. & Minor, W. (1997). *Methods Enzymol.* **276**, 307–326.
Seals, D. F. & Courtneidge, S. A. (2003). *Genes Dev.* **17**, 7–30.
Takeda, S., Igarashi, T., Mori, H. & Araki, S. (2006). *EMBO J.* **25**, 2388–2396.
Trummal, K., Tonismagi, K., Siigur, E., Aaspollu, A., Lopp, A., Sillat, T., Saat, R., Kasak, L., Tammiste, I., Kogerman, P., Kalkkinen, N. & Siigur, J. (2005). *Toxicon*, **46**, 46–61.
White, J. M. (2003). *Curr. Opin. Cell Biol.* **15**, 598–606.
You, W. K., Seo, H. J., Chung, K. H. & Kim, D. S. (2003). *J. Biochem. (Tokyo)*, **134**, 739–749.

Am J Physiol Heart Circ Physiol 291: H2187–H2191, 2006.
First published June 9, 2006; doi:10.1152/ajpheart.00175.2006.

Effects of Ca^{2+} channel antagonists on nerve stimulation-induced and ischemia-induced myocardial interstitial acetylcholine release in cats

Toru Kawada,[1] Toji Yamazaki,[2] Tsuyoshi Akiyama,[2] Kazunori Uemura,[1] Atsunori Kamiya,[1] Toshiaki Shishido,[1] Hidezo Mori,[2] and Masaru Sugimachi[1]

[1]*Department of Cardiovascular Dynamics, Advanced Medical Engineering Center, National Cardiovascular Center Research Institute and* [2]*Department of Cardiac Physiology, National Cardiovascular Center Research Institute, Osaka, Japan*

Submitted 17 February 2006; accepted in final form 7 June 2006

Kawada, Toru, Toji Yamazaki, Tsuyoshi Akiyama, Kazunori Uemura, Atsunori Kamiya, Toshiaki Shishido, Hidezo Mori, and Masaru Sugimachi. Effects of Ca^{2+} channel antagonists on nerve stimulation-induced and ischemia-induced myocardial interstitial acetylcholine release in cats. *Am J Physiol Heart Circ Physiol* 291: H2187–H2191, 2006. First published June 9, 2006; doi:10.1152/ajpheart.00175.2006.—Although an axoplasmic Ca^{2+} increase is associated with an exocytotic acetylcholine (ACh) release from the parasympathetic postganglionic nerve endings, the role of voltage-dependent Ca^{2+} channels in ACh release in the mammalian cardiac parasympathetic nerve is not clearly understood. Using a cardiac microdialysis technique, we examined the effects of Ca^{2+} channel antagonists on vagal nerve stimulation- and ischemia-induced myocardial interstitial ACh releases in anesthetized cats. The vagal stimulation-induced ACh release [22.4 nM (SD 10.6), $n = 7$] was significantly attenuated by local administration of an N-type Ca^{2+} channel antagonist ω-conotoxin GVIA [11.7 nM (SD 5.8), $n = 7$, $P = 0.0054$], or a P/Q-type Ca^{2+} channel antagonist ω-conotoxin MVIIC [3.8 nM (SD 2.3), $n = 6$, $P = 0.0002$] but not by local administration of an L-type Ca^{2+} channel antagonist verapamil [23.5 nM (SD 6.0), $n = 5$, $P = 0.758$]. The ischemia-induced myocardial interstitial ACh release [15.0 nM (SD 8.3), $n = 8$] was not attenuated by local administration of the L-, N-, or P/Q-type Ca^{2+} channel antagonists, by inhibition of Na^+/Ca^{2+} exchange, or by blockade of inositol 1,4,5-trisphosphate [Ins(1,4,5)P_3] receptor but was significantly suppressed by local administration of gadolinium [2.8 nM (SD 2.6), $n = 6$, $P = 0.0283$]. In conclusion, stimulation-induced ACh release from the cardiac postganglionic nerves depends on the N- and P/Q-type Ca^{2+} channels (with a dominance of P/Q-type) but probably not on the L-type Ca^{2+} channels in cats. In contrast, ischemia-induced ACh release depends on nonselective cation channels or cation-selective stretch activated channels but not on L-, N-, or P/Q type Ca^{2+} channels, Na^+/Ca^{2+} exchange, or Ins(1,4,5)P_3 receptor-mediated pathway.

cardiac microdialysis; ω-conotoxin GVIA; ω-conotoxin MVIIC; KB-R7943; verapamil; vagal stimulation

ALTHOUGH N-TYPE Ca^{2+} CHANNELS play a dominant role in norepinephrine release from sympathetic nerve endings (8, 33, 34), the type(s) of Ca^{2+} channels controlling ACh release in the mammalian parasympathetic system is not fully understood and show diversity among reports. To name a few, in isolated parasympathetic submandibular ganglia from the rat, neurotransmission is mediated by Ca^{2+} channels that are resistant to the L-, N-, P/Q-, and R- type Ca^{2+} channel antagonists (29). When the negative inotropic response to field stimulation was examined in the isolated guinea pig atria, Hong and Chang (8) reported the importance of P/Q-type Ca^{2+} channels, whereas Serone et al. (28) reported the importance of N-type Ca^{2+} channels. Because field stimulation in the isolated preparations could induce responses different from those in the in vivo conditions, we aimed to examine the effects of Ca^{2+} channel antagonists on the vagal nerve stimulation-induced myocardial interstitial ACh release in the in vivo feline heart.

Aside from the important role of the normal physiological regulation of the heart, the vagal nerve can be a therapeutic target for certain cardiovascular diseases (2, 3, 13, 22, 27). In previous studies, we have shown that acute myocardial ischemia causes myocardial interstitial ACh release in the ischemic region independently of efferent vagal nerve activity (12, 14). The comparison of the effects of Ca^{2+} channel antagonists on the ACh releases induced by vagal nerve stimulation and by acute myocardial ischemia may deepen our understanding about the ischemia-induced myocardial interstitial ACh release.

A cardiac microdialysis technique offers detailed analyses of in vivo myocardial interstitial ACh release (1, 15). Because the local administration of pharmacological agents through a dialysis probe can modulate ACh release without significantly affecting systemic hemodynamics, a combination of cardiac microdialysis with local pharmacological interventions is useful for analyzing the mechanisms of ACh release in vivo. In the present study, we examined the effects of Ca^{2+} channel antagonists on nerve stimulation- and ischemia-induced ACh releases in anesthetized cats. The results indicate that stimulation-induced ACh release from the cardiac parasympathetic postganglionic nerves depends on the N- and P/Q-type Ca^{2+} channels but probably not on the L-type Ca^{2+} channels. In contrast, ischemia-induced myocardial interstitial ACh release is resistant to the inhibition of L-, N-, and P/Q-type Ca^{2+} channels. In addition, the ischemia-induced myocardial ACh release is resistant to the inhibition of Na^+/Ca^{2+} exchanger and the blockade of inositol 1,4,5-trisphosphate [Ins(1,4,5)P_3] receptor but is suppressed by gadolinium, suggesting that nonselective cation channels or cation-selective stretch-activated channels are involved.

MATERIALS AND METHODS

Common Preparation

Animal care was provided in accordance with the *Guiding Principles for the Care and Use of Animals in the Field of Physiological*

Address for reprint requests and other correspondence: T. Kawada, Dept. of Cardiovascular Dynamics, Advanced Medical Engineering Center, National Cardiovascular Center Research Institute, 5-7-1 Fujishirodai, Suita, Osaka 565-8565, Japan (e-mail: torukawa@res.ncvc.go.jp).

The costs of publication of this article were defrayed in part by the payment of page charges. The article must therefore be hereby marked "*advertisement*" in accordance with 18 U.S.C. Section 1734 solely to indicate this fact.

Sciences approved by the Physiological Society of Japan. All protocols were approved by the Animal Subjects Committee of the National Cardiovascular Center. Adult cats weighing from 2.2 to 4.2 kg were anesthetized via an intraperitoneal injection of pentobarbital sodium (30–35 mg/kg) and ventilated mechanically with room air mixed with oxygen. The depth of anesthesia was maintained with a continuous intravenous infusion of pentobarbital sodium (1–2 mg·kg^{-1}·h^{-1}) through a catheter inserted from the right femoral vein. Systemic arterial pressure was monitored from a catheter inserted from the right femoral artery. The vagi were sectioned bilaterally at the neck. The esophageal temperature of the animal, which was measured by a thermometer (CTM-303, TERUMO, Japan), was maintained at around 37°C using a heated pad and a lamp.

With the animal in the lateral position, the left fifth and sixth ribs were resected to expose the heart. A dialysis probe was implanted transversely, using a fine guiding needle, into the anterolateral free wall of the left ventricle perfused by the left anterior descending coronary artery (LAD). Heparin sodium (100 U/kg) was administered intravenously to prevent blood coagulation. At the end of the experiment, the experimental animals were killed with an overdose of pentobarbital sodium. Postmortem examination confirmed that the dialysis probe had been threaded in the middle layer of the left ventricular myocardium. The thickness of the left ventricular free wall was ~7–8 mm, and the semipermeable membrane of the dialysis probe was positioned ~3–4 mm from the epicardial surface.

Dialysis Technique

The materials and properties of the dialysis probe have been described previously (1). Briefly, we designed a transverse dialysis probe. A dialysis fiber of semipermeable membrane (13 mm length, 310 μm OD, 200 μm ID; PAN-1200, 50,000 molecular weight cutoff, Asahi Chemical, Japan) was glued at both ends to polyethylene tubes (25 cm length, 500 μm OD, 200 μm ID). The dialysis probe was perfused at a rate of 2 μl/min with Ringer solution containing a cholinesterase inhibitor eserine (physostigmine, 100 μM). Experimental protocols were started 2 h after the dialysis probe was implanted when the ACh concentration in the dialysate reached a steady state. The ACh concentration in the dialysate was measured by high-performance liquid chromatography with electrochemical detection (Eicom, Kyoto, Japan).

Local administration of a pharmacological agent was carried out through a dialysis probe. That is to say, we added the pharmacological agent to the perfusate and allowed 1 h for a settling time. The pharmacological agent should spread around the semipermeable membrane, thereby affecting the neurotransmitter release in the vicinity of the semipermeable membrane. Because the distribution across the semipermeable membrane is required, based on previous results (33, 34), we used the pharmacological agent at the concentration 10–100 times higher than that required for complete channel blockade in experimental settings in vitro.

Specific Preparation and Protocols

Protocol 1. Bipolar platinum electrodes were attached bilaterally to the cardiac ends of the sectioned vagi at the neck. The nerves and electrodes were covered with warmed mineral oil for insulation. The vagal nerves were stimulated for 15 min (20 Hz, 1 ms, 10 V). We measured the stimulation-induced ACh release in the absence of Ca^{2+} channel blockade (control, $n = 7$) and examined the effects of an L-type Ca^{2+} channel antagonist verapamil (100 μM, $n = 5$), an N-type Ca^{2+} channel antagonist ω-conotoxin GVIA (10 μM, $n = 7$), a P/Q-type Ca^{2+} channel antagonist ω-conotoxin MVIIC (10 μM, $n = 6$), and combined administration of ω-conotoxin GVIA and ω-conotoxin MVIIC (10 μM each, $n = 6$).

Protocol 2. Because a preliminary result from *protocol 1* suggested that local administration of verapamil was ineffective in suppressing stimulation-induced ACh release, we examined the effects of the intravenous administration of verapamil (300 μg/kg, $n = 6$) on stimulation-induced ACh release in vagotomized animals as a supplemental experiment.

Protocol 3. A 60-min LAD occlusion was performed by using a 3-0 silk suture passed around the LAD just distal to the first diagonal branch. We measured the ACh levels during 45–60 min of ischemia in the absence of Ca^{2+} channel blockade (control, $n = 8$) and examined the effects of verapamil (100 μM, $n = 5$), ω-conotoxin GVIA (10 μM, $n = 5$), and ω-conotoxin MVIIC (10 μM, $n = 5$). A previous result indicated that the ischemia-induced ACh release reached the steady state during 45–60 min of ischemia (14). We also examined the effects of three additional agents, a Na^+/Ca^{2+} exchange inhibitor KB-R7943 (10 μM, $n = 5$) (9, 10), an Ins(1,4,5)P_3 receptor blocker xestospongin C (500 μM, $n = 6$) (25), and a nonselective cation channel blocker or a cation-selective stretch activated channel blocker gadolinium (1 mM) (5, 17), on the ischemia-induced ACh release.

Statistical Analysis

All data are presented as mean (SD) values. In *protocol 1*, we compared stimulation-induced ACh release among the five groups using one-way analysis of variance followed by the Student-Neuman-Keuls test (6). In *protocol 2*, we used an unpaired-*t* test (two-sided) to examine the effect of intravenous verapamil administration on stimulation-induced ACh release. In *protocol 3*, we compared ischemia-induced ACh release among the seven groups using one-way analysis of variance followed by the Dunnett' test against the control. For all analyses, differences were considered significant when $P < 0.05$.

RESULTS

In *protocol 1*, the ACh level during electrical vagal stimulation was 22.4 nM (SD 10.6). Local administration of verapamil did not affect stimulation-induced ACh release (Fig. 1). In contrast, local administration of ω-conotoxin GVIA or ω-conotoxin MVIIC suppressed stimulation-induced ACh release. The extent of suppression was greater in the latter. The ACh level was significantly lower in the simultaneous administration group (ω-conotoxin GVIA + ω-conotoxin MVIIC)

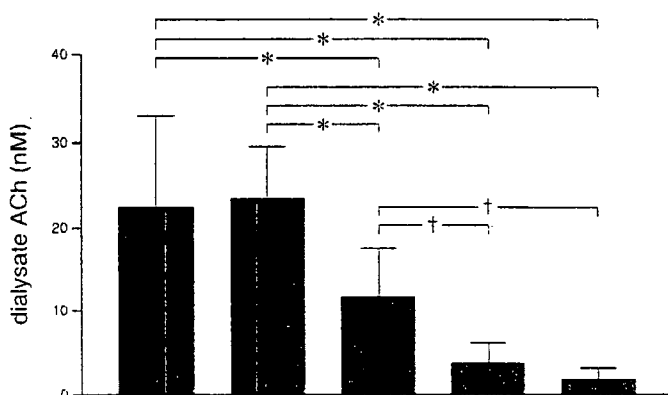

	vehicle	verapamil	ω-CTX GVIA	ω-CTX MVIIC	ω-CTX MVIIC + ω-CTX GVIA
vehicle		0.758	*0.0054*	*0.0002*	*0.0002*
verapamil	0.758		*0.0066*	*0.0002*	*0.0001*
GVIA	*0.0054*	*0.0066*		*0.033*	*0.025*
MVIIC	*0.0002*	*0.0002*	*0.033*		0.581
MVIIC+GVIA	*0.0002*	*0.0001*	*0.025*	0.581	

Fig. 1. Effects of local administration of verapamil, ω-conotoxin GVIA, ω-conotoxin MVIIC, or ω-conotoxin GVIA plus ω-conotoxin MVIIC on vagal nerve stimulation-induced myocardial interstitial ACh release. Both ω-conotoxin GVIA and ω-conotoxin MVIIC, but not verapamil, suppressed stimulation-induced ACh release. Data are mean (SD) values. *$P < 0.01$, †$P < 0.05$. The exact P values are presented.

than that in the ω-conotoxin GVIA group but was not different from the ω-conotoxin MVIIC group.

In *protocol 2*, the intravenous administration of verapamil did not significantly change stimulation-induced ACh release [21.7 nM (SD 12.8)] compared with the control group (P = 0.91).

In *protocol 3*, the ACh level in the ischemic region was 14.9 nM (SD 8.3) during 45–60 min of acute myocardial ischemia. Inhibition of voltage-dependent Ca^{2+} channels by local administration of verapamil, ω-conotoxin GVIA, or ω-conotoxin MVIIC did not affect ischemia-induced ACh release (Fig. 2). Inhibition of the reverse mode action of Na^{+}/Ca^{2+} exchange by local administration of KB-R7943 appeared to have augmented rather than suppressed ischemia-induced ACh release, though there was no statistically significant difference from the control. Blockade of the Ins(1,4,5)P_3 receptor by local administration of xestospongin C did not affect the ischemia-induced ACh release. In contrast, blockade of nonselective cation channels or cation-selective stretch-activated channels by local administration of gadolinium suppressed the ischemia-induced ACh release.

DISCUSSION

Ca^{2+} Channels Involved in Stimulation-Induced ACh Release

Although neurotransmitter release at mammalian sympathetic neuroeffector junctions predominantly depends on Ca^{2+} influx through N-type Ca^{2+} channels (23, 33, 34), the type(s) of Ca^{2+} channels involved in ACh release from cardiac parasympathetic neuroeffector junctions show diversity among reports (8, 28). One possible factor hampering investigations into parasympathetic postganglionic neurotransmitter release in response to vagal nerve stimulation in vivo is that the parasympathetic ganglia are usually situated in the vicinity of the effector organs, thereby making it difficult to separately assess ACh release from preganglionic and postganglionic nerves. In the previous study from our laboratory, intravenous administration, but not local administration of a ganglionic blocker, hexamethonium reduced vagal stimulation-induced ACh release assessed by cardiac microdialysis (1). The negligible effect of local hexamethonium administration on stimulation-induced ACh release suggests the lack of parasympathetic ganglia around the dialysis probe. In support of our speculation, a recent neuroanatomical finding indicates that three ganglia, away from the left anterior free wall targeted by the dialysis probe, provide the major source for left ventricular postganglionic innervation in cats: a cranioventricular ganglion, a left ventricular ganglion 2 (so designated), and an interventriculo-septal ganglion (11). Therefore, ACh, as measured by cardiac microdialysis, is considered to predominantly reflect ACh release from parasympathetic postganglionic nerves.

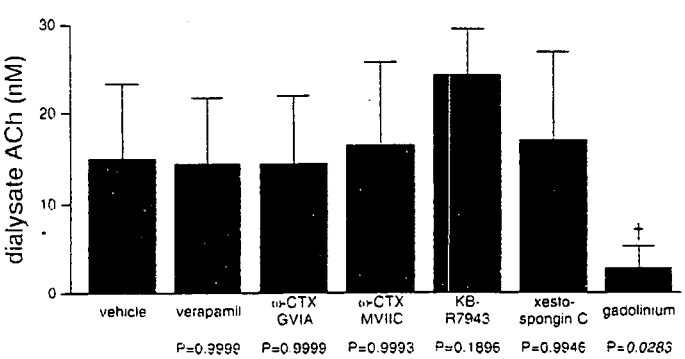

Fig. 2. Effects of local administration of verapamil, ω-conotoxin GVIA, ω-conotoxin MVIIC, KB-R7943, xestospongin C, or gadolinium on acute myocardial ischemia-induced myocardial interstitial ACh release in the ischemic region. Gadolinium alone suppressed the ischemia-induced ACh release. Data are mean (SD) values. †P < 0.05. The exact P values are presented.

Local (*protocol 1*) or intravenous (*protocol 2*) administration of verapamil did not affect stimulation-induced ACh release. In contrast, vagal stimulation-induced ACh release was reduced in both the ω-conotoxin GVIA and ω-conotoxin MVIIC groups but to a greater extent in the latter (Fig. 1). Therefore, both N- and P/Q-type, but probably not L-type, Ca^{2+} channels are involved in stimulation-induced ACh release from the cardiac parasympathetic postganglionic nerves in cats. The contribution of P/Q type Ca^{2+} channels to ACh release might be greater than that of N-type Ca^{2+} channels. Hong and Chang (8) reported that the negative inotropic response to field stimulation depends predominantly on the P/Q-type Ca^{2+} channels in isolated guinea pig atria, whereas Serone et al. (28) reported the predominance of N-type Ca^{2+} channels. In those studies, the field stimulation employed differed from ordinary activation of the postganglonic nerves by nerve discharge and, in addition, ACh release was not directly measured. The present study directly demonstrated the involvement of P/Q- and N-type Ca^{2+} channels in the stimulation-induced ACh release in the cardiac parasympathetic postganglionic nerves. These results support the concept that multiple subtypes of the voltage-gated Ca^{2+} channel mediate transmitter release from the same population of parasympathetic neurons (31).

Stimulation-induced ACh release was suppressed by ~50% in the ω-conotoxin GVIA group and by ~80% in the ω-conotoxin MVIIC group. The algebraic summation of the extent of suppression exceeded 100%. The phenomenon may be in part due to the nonlinear dose-response relationship between Ca^{2+} influx and transmitter release (32). The supra-additive phenomenon may be also due to the affinity of ω-conotoxin MVIIC to N-type Ca^{2+} channels (8, 26, 36). Combined local administration of ω-conotoxin GVIA and ω-conotoxin MVIIC almost completely suppressed stimulation-induced ACh release to a level similar to that achieved by the Na^{+} channel inhibitor tetrodotoxin (15). Therefore, involvement of another untested type of Ca^{2+} channel(s) is unlikely in the stimulation-induced ACh release from the cardiac parasympathetic postganglionic nerves in cats.

Ca^{2+} Channels and Ischemia-Induced ACh Release

In a previous study, we showed that acute myocardial ischemia evokes myocardial interstitial ACh release in the ischemic region via a local mechanism independent of efferent vagal nerve activity (14). In that study, the inhibition of intracellular Ca^{2+} mobilization by local administration of 3,4,5-trimethoxybenzoic acid 8-(diethyl amino)-octyl ester (TMB-8) suppressed ischemia-induced ACh release, suggesting that an axoplasmic Ca^{2+} elevation is essential for the ischemia-induced ACh release. Because tissue K^{+} concentration increases in the ischemic region (7, 18), high K^{+}-induced

depolarization could activate voltage-dependent Ca^{2+} channels even in the absence of efferent vagal nerve activity. However, ischemia-induced ACh release was not suppressed by local administration of verapamil, ω-conotoxin GVIA, or ω-conotoxin MVIIC (Fig. 2). Therefore, Ca^{2+} entry through the voltage-dependent Ca^{2+} channels is unlikely a mechanism for the ischemia-induced myocardial interstitial ACh release.

Acute myocardial ischemia causes energy depletion in the ischemic region, which impairs Na^+-K^+-ATPase activity. Ischemia also causes acidosis in the ischemic region, which promotes Na^+/H^+ exchange. As a result, ischemia causes intracellular Na^+ accumulation. The decrease in the Na^+ gradient across the plasma membrane may then cause the Na^+/Ca^{2+} exchanger to operate in the reverse mode, facilitating intracellular Ca^{2+} overload. KB-R7943 can inhibit the reverse mode of Na^+/Ca^{2+} exchange (9, 10) and its potential to protect against ischemia-reperfusion injury has been reported (21). In the present study, however, local administration of KB-R7943 failed to suppress and rather increased ACh release during ischemia as opposed to our expectation. It is plausible that the inhibition of reverse mode of Na^+/Ca^{2+} may have facilitated the accumulation of intracellular Na^+ and induced adverse effects that cancelled the possible beneficial effects derived from the inhibition of Ca^{2+} entry through the Na^+/Ca^{2+} exchanger itself. In addition, KB-R7943 could inhibit the forward mode of Na^+/Ca^{2+} exchange and reduce Ca^{2+} efflux (16), contributing to the intracellular Ca^{2+} accumulation and ACh release. In the present study, we observed the effects of KB-R7943 only during the ischemic period. However, accumulation of intracellular Na^+ through Na^+/H^+ exchange is enhanced on reperfusion due to the washout of extracellular H^+ (20). The inhibition of Na^+/Ca^{2+} exchange to suppress Ca^{2+} overload might become more important during the reperfusion phase. For instance, the percent segment shortening of the left ventricle was improved by KB-R7943 during reperfusion but not during ischemia (35).

As already mentioned, the ischemia-induced ACh release can be blocked by TMB-8 and thus the intracellular Ca^{2+} mobilization is required for the ischemia-induced ACh release (14). Besides the Ca^{2+} entries through voltage-dependent Ca^{2+} channels and via the reverse mode of Na^+/Ca^{2+} exchanger, Ca^{2+} may be mobilized from the endoplasmic reticulum via pathological pathways. As an example, the mitochondrial permeability transition pore triggered in pathological conditions is linked to cytochrome c release. Cytochrome c can bind to the endoplasmic reticulum $Ins(1,4,5)P_3$ receptor, rendering the channel insensitive to autoinhibition by high cytosolic Ca^{2+} concentration and resulting in enhanced endoplasmic reticulum Ca^{2+} release (4, 30). In the present study, however, blockade of $Ins(1,4,5)P_3$ receptor by xestospongin C failed to suppress the ischemia-induced ACh release. In contrast, local administration of gadolinium significantly suppressed the ischemia-induced ACh release. Therefore, nonselective cation channels or cation-selective stretch-activated channels contribute to the ischemia-induced ACh release. During myocardial ischemia, the ischemic region can be subjected to paradoxical systolic bulging. Such bulging likely opens stretch-activated channels and causes myocardial interstitial ACh release, possibly leading to cardioprotection by ACh against ischemic injury (2).

Limitations

First, the experiment was performed under anesthetic conditions, which may have influenced basal autonomic activity. However, because we sectioned the vagi at the neck, basal autonomic activity may have had only a minor effect on ACh release during the vagal stimulation and during acute myocardial ischemia. Second, we added eserine to the perfusate to inhibit immediate degradation of ACh (24), which may have increased the ACh level in the synaptic cleft and activated regulatory pathways such as autoinhibition of ACh release via muscarinic receptors (24). However, the myocardial interstitial ACh level measured under this condition could reflect changes induced by Na^+ channel inhibitor, choline uptake inhibitor, and vesicular ACh transport inhibitor as described in a previous study (15). Therefore, we think that the interpretation of the present results is reasonable. Third, tissue and species differences should be taken into account when extrapolating the present findings, because significant heterogeneity in the Ca^{2+} channels involved in the mammalian parasympathetic system may exist. Finally, we used verapamil to test the involvement of L-type Ca^{2+} channels in the ACh release. There are three major types of L-type Ca^{2+} channel antagonists with different binding domains (verapamil, nifedipine, and diltiazem) (19). Whether the effects on the ACh release are common among the three types of L-type Ca^{2+} channel antagonists remains unanswered.

In conclusion, the N- and P/Q-type Ca^{2+} channels (with the P/Q-type dominant), but probably not the L-type Ca^{2+} channels, are involved in vagal stimulation-induced ACh release from the cardiac parasympathetic postganglionic nerves in cats. In contrast, myocardial interstitial ACh release in the ischemic myocardium is resistant to the blockade of L-, N-, and P/Q-type Ca^{2+} channels. In addition, the ischemia-induced myocardial ACh release is resistant to the inhibition of Na^+/Ca^{2+} exchanger and the blockade of $Ins(1,4,5)P_3$ receptor but is suppressed by gadolinium, suggesting that nonselective cation channels or cation-selective stretch-activated channels are involved.

GRANTS

This study was supported by Health and Labour Sciences Research Grant for Research on Advanced Medical Technology from the Ministry of Health, Labour and Welfare of Japan, Health and Labour Sciences Research Grant for Research on Medical Devices for Analyzing, Supporting and Substituting the Function of Human Body from the Ministry of Health, Labour and Welfare of Japan, Health and Labour Sciences Research Grant H18-Iryo-Ippan-023 from the Ministry of Health, Labour and Welfare of Japan, Program for Promotion of Fundamental Studies in Health Science from the National Institute of Biomedical Innovation, a Grant provided by the Ichiro Kanehara Foundation, Ground-based Research Announcement for Space Utilization promoted by Japan Space Forum, and Industrial Technology Research Grant Program in 03A47075 from New Energy and Industrial Technology Development Organization of Japan.

REFERENCES

1. **Akiyama T, Yamazaki T, and Ninomiya I.** In vivo detection of endogenous acetylcholine release in cat ventricles. *Am J Physiol Heart Circ Physiol* 266: H854–H860, 1994.
2. **Ando M, Katare RG, Kakinuma Y, Zhang D, Yamasaki F, Muramoto K, and Sato T.** Efferent vagal nerve stimulation protects heart against ischemia-induced arrhythmias by preserving connexin43 protein. *Circulation* 112: 164–170, 2005.

3. **Bibevski S and Dunlap ME.** Prevention of diminished parasympathetic control of the heart in experimental heart failure. *Am J Physiol Heart Circ Physiol* 287: H1780–H1785, 2004.
4. **Brookes PS, Yoon Y, Robotham JL, Anders MW, and Sheu SS.** Calcium, ATP, and ROS: a mitochondrial love-hate triangle. *Am J Physiol Cell Physiol* 287: C817–C833, 2004.
5. **Caldwell RA, Clemo HF, and Baumgarten CM.** Using gadolinium to identify stretch-activated channels: technical considerations. *Am J Physiol Cell Physiol* 275: C619–C621, 1998.
6. **Glantz SA.** *Primer of Biostatistics* (5th ed) New York: McGraw-Hill, 2002.
7. **Hirche HJ, Franz CHR, Bös L, Bissig R, Lang R, and Schramm M.** Myocardial extracellular K^+ and H^+ increase and noradrenaline release as possible cause of early arrhythmias following acute coronary artery occlusion in pigs. *J Mol Cell Cardiol* 12: 579–593, 1979.
8. **Hong SJ and Chang CC.** Calcium channel subtypes for the sympathetic and parasympathetic nerves of guinea-pig atria. *Br J Pharmacol* 116: 1577–1582, 1995.
9. **Iwamoto T, Kita S, Uehara A, Inoue Y, Taniguchi Y, Imanaga I, and Shigekawa M.** Structural domains influencing sensitivity to isothiourea derivative inhibitor KB-R7943 in cardiac Na^+/Ca^{2+} exchanger. *Mol Pharmacol* 59: 524–531, 2001.
10. **Iwamoto T, Watano T, and Shigekawa M.** A novel isothiourea derivative selectively inhibits the reverse mode of Na^+/Ca^{2+} exchange in cells expressing NCX1. *J Biol Chem* 271: 22391–22397, 1996.
11. **Johnson TA, Gray AL, Lauenstein JM, Newton SS, and Massari VJ.** Parasympathetic control of the heart. I. An interventriculo-septal ganglion is the major source of the vagal intracardiac innervation of the ventricles. *J Appl Physiol* 96: 2265–2272, 2004.
12. **Kawada T, Yamazaki T, Akiyama T, Inagaki M, Shishido T, Zheng C, Yanagiya Y, Sugimachi M, and Sunagawa K.** Vagosympathetic interactions in ischemia-induced myocardial norepinephrine and acetylcholine release. *Am J Physiol Heart Circ Physiol* 280: H216–H221, 2001.
13. **Kawada T, Yamazaki T, Akiyama T, Li M, Ariumi H, Mori H, Sunagawa K, and Sugimachi M.** Vagal stimulation suppresses ischemia-induced myocardial interstitial norepinephrine release. *Life Sci* 78: 882–887, 2006.
14. **Kawada T, Yamazaki T, Akiyama T, Sato T, Shishido T, Inagaki M, Takaki H, Sugimachi M, and Sunagawa K.** Differential acetylcholine release mechanisms in the ischemic and non-ischemic myocardium. *J Mol Cell Cardiol* 32: 405–414, 2000.
15. **Kawada T, Yamazaki T, Akiyama T, Shishido T, Inagaki M, Uemura K, Miyamoto T, Sugimachi M, Takaki H, and Sunagawa K.** In vivo assessment of acetylcholine-releasing function at cardiac vagal nerve terminals. *Am J Physiol Heart Circ Physiol* 281: H139–H145, 2001.
16. **Kimura J, Watano T, Kawahara M, Sakai E, and Yatabe J.** Direction-independent block of bi-directional Na^+/Ca^{2+} exchange current by KB-R7943 in guinea-ping cardiac myocytes. *Br J Pharmacol* 128: 969–974, 1999.
17. **Kimura S, Mieno H, Tamaki K, Inoue M, and Chayama K.** Nonselective cation channel as a Ca^{2+} influx pathway in pepsinogen-secreting cells of bullfrog esophagus. *Am J Physiol Gastrointest Liver Physiol* 281: G333–G341, 2001.
18. **Kléber AG.** Extracellular potassium accumulation in acute myocardial ischemia. *J Mol Cell Cardiol* 16: 389–394, 1984.
19. **Kurokawa J, Adachi-Akahane S, and Nagao T.** 1,5-Benzothiazepine binding domain is located on the extracellular side of the cardiac L-type Ca^{2+} channel. *Mol Pharmacol* 51: 262–268, 1997.
20. **Lazdunski M, Frelin C, and Vigne P.** The sodium/hydrogen exchange system in cardiac cells: its biochemical and pharmacological properties and its role in regulating internal concentrations of sodium and internal pH. *J Mol Cell Cardiol* 17: 1029–1042, 1985.
21. **Lee C, Dhalla NS, and Hryshko LV.** Therapeutic potential of novel Na^+-Ca^{2+} exchange inhibitors in attenuating ischemia-reperfusion injury. *Can J Cardiol* 21: 509–516, 2005.
22. **Li M, Zheng C, Sato T, Kawada T, Sugimachi M, and Sunagawa K.** Vagal nerve stimulation markedly improves long-term survival after chronic heart failure in rats. *Circulation* 109: 120–124, 2004.
23. **Molderings GJ, Likungu J, and Göthert M.** N-type calcium channels control sympathetic neurotransmission in human heart atrium. *Circulation* 101: 403–407, 2000.
24. **Nicholls DG.** *Proteins, Transmitters and Synapses*. Oxford: Blackwell Science, 1994.
25. **Oka T, Sato K, Hori M, Ozaki H, and Karaki H.** Xestospongin C, a novel blocker of IP_3 receptor, attenuates the increase in cytosolic calcium level and degranulation that is induced by antigen in RBL-2H3 mast cells. *Br J Pharmacol* 135: 1959–1966, 2002.
26. **Randall A and Tsien RW.** Pharmacological dissection of multiple types of Ca^{2+} channel currents in rat cerebellar granule neurons. *J Neurosci* 15: 2995–3012, 1995.
27. **Schauerte P, Scherlag BJ, Scherlag MA, Goli S, Jackman WM, and Lazzara R.** Ventricular rate control during atrial fibrillation by cardiac parasympathetic nerve stimulation: a transvenous approach. *J Am Coll Cardiol* 34: 2043–2050, 1999.
28. **Serone AP and Angus JA.** Role of N-type calcium channels in autonomic neurotransmission in guinea-pig isolated left atria. *Br J Pharmacol* 127: 927–934, 1999.
29. **Smith AB, Motin L, Lavidis NA, and Adams DJ.** Calcium channels controlling acetylcholine release from preganglionic nerve terminals in rat autonomic ganglia. *Neuroscience* 95: 1121–1127, 2000.
30. **Verkhratsky A and Toescu EC.** Endoplasmic reticulum Ca^{2+} homeostasis and neuronal death. *J Cell Mol Med* 4: 351–361, 2003.
31. **Waterman SA.** Multiple subtypes of voltage-gated calcium channel mediate transmitter release from parasympathetic neurons in the mouse bladder. *J Neurosci* 16: 4155–4161, 1996.
32. **Wheeler DB, Randall A, and Tsien RW.** Changes in action potential duration after reliance of excitatory synaptic transmission on multiple types of Ca^{2+} channels in rat hippocampus. *J Neurosci* 16: 2226–2237, 1996.
33. **Yahagi N, Akiyama T, and Yamazaki T.** Effects of ω-conotoxin GVIA on cardiac sympathetic nerve function. *J Auton Nerv Syst* 68: 43–48, 1998.
34. **Yamazaki T, Akiyama T, Kitagawa H, Takauchi Y, Kawada T, and Sunagawa K.** A new, concise dialysis approach to assessment of cardiac sympathetic nerve terminal abnormalities. *Am J Physiol Heart Circ Physiol* 272: H1182–H1187, 1997.
35. **Yoshitomi O, Akiyama D, Hara T, Cho S, Tomiyasu S, and Sumikawa K.** Cardioprotective effects of KB-R7943, a novel inhibitor of Na^+/Ca^{2+} exchanger, on stunned myocardium in anesthetized dogs. *J Anesth* 19: 124–130, 2005.
36. **Zhang JF, Randall AD, Ellinor PT, Horne WA, Sather WA, Tanabe T, Schwarz TL, and Tsien RW.** Distinctive pharmacology and kinetics of cloned neuronal Ca^{2+} channels and their possible counterparts in mammalian CNS neurons. *Neuropharmacology* 32: 1075–1088, 1993.

Am J Physiol Heart Circ Physiol 291: H1138–H1146, 2006.
First published April 28, 2006; doi:10.1152/ajpheart.00187.2006.

Cardioprotective role of endogenous hydrogen peroxide during ischemia-reperfusion injury in canine coronary microcirculation in vivo

Toyotaka Yada,[1] Hiroaki Shimokawa,[3] Osamu Hiramatsu,[1] Yoshisuke Haruna,[2] Yoshitaka Morita,[2] Naoki Kashihara,[2] Yoshiro Shinozaki,[4] Hidezo Mori,[5] Masami Goto,[1] Yasuo Ogasawara,[1] and Fumihiko Kajiya[1]

[1]*Department of Medical Engineering and Systems Cardiology and* [2]*Division of Nephrology and Rheumatology, Department of Internal Medicine, Kawasaki Medical School, Kurashiki;* [3]*Department of Cardiovascular Medicine, Tohoku University Graduate School of Medicine, Sendai;* [4]*Department of Physiology, Tokai University School of Medicine, Isehara; and* [5]*Department of Cardiac Physiology, National Cardiovascular Center Research Institute, Suita, Japan*

Submitted 22 February 2006; accepted in final form 18 April 2006

Yada, Toyotaka, Hiroaki Shimokawa, Osamu Hiramatsu, Yoshisuke Haruna, Yoshitaka Morita, Naoki Kashihara, Yoshiro Shinozaki, Hidezo Mori, Masami Goto, Yasuo Ogasawara, and Fumihiko Kajiya. Cardioprotective role of endogenous hydrogen peroxide during ischemia-reperfusion injury in canine coronary microcirculation in vivo. *Am J Physiol Heart Circ Physiol* 291: H1138–H1146, 2006. First published April 28, 2006; doi:10.1152/ajpheart.00187.2006.—We have recently demonstrated that endogenous H_2O_2 plays an important role in coronary autoregulation in vivo. However, the role of H_2O_2 during coronary ischemia-reperfusion (I/R) injury remains to be examined. In this study, we examined whether endogenous H_2O_2 also plays a protective role in coronary I/R injury in dogs in vivo. Canine subepicardial small coronary arteries (≥100 μm) and arterioles (<100 μm) were continuously observed by an intravital microscope during coronary I/R (90/60 min) under cyclooxygenase blockade (n = 50). Coronary vascular responses to endothelium-dependent vasodilators (ACh) were examined before and after I/R under the following seven conditions: control, nitric oxide (NO) synthase (NOS) inhibitor N^G-monomethyl-L-arginine (L-NMMA), catalase (a decomposer of H_2O_2), 8-sulfophenyltheophylline (8-SPT, an adenosine receptor blocker), L-NMMA + catalase, L-NMMA + tetraethylammonium (TEA, an inhibitor of large-conductance Ca^{2+}-sensitive potassium channels), and L-NMMA + catalase + 8-SPT. Coronary I/R significantly impaired the coronary vasodilatation to ACh in both sized arteries (both $P < 0.01$); L-NMMA reduced the small arterial vasodilatation (both $P < 0.01$), whereas it increased ($P < 0.05$) the ACh-induced coronary arteriolar vasodilatation associated with fluorescent H_2O_2 production after I/R. Catalase increased the small arterial vasodilatation ($P < 0.01$) associated with fluorescent NO production and increased endothelial NOS expression, whereas it decreased the arteriolar response after I/R ($P < 0.01$). L-NMMA + catalase, L-NMMA + TEA, or L-NMMA + catalase + 8-SPT further decreased the coronary vasodilatation in both sized arteries (both, $P < 0.01$). L-NMMA + catalase, L-NMMA + TEA, and L-NMMA + catalase + 8-SPT significantly increased myocardial infarct area compared with the other four groups (control, L-NMMA, catalase, and 8-SPT; all, $P < 0.01$). These results indicate that endogenous H_2O_2, in cooperation with NO, plays an important cardioprotective role in coronary I/R injury in vivo.

endothelium-derived relaxing factor; myocardial infarction; vascular endothelial function

VASCULAR ENDOTHELIAL CELLS play an important role in maintaining vascular homeostasis by synthesizing and releasing endothelium-derived relaxing factors (EDRFs), including prostacyclin (PGI_2), nitric oxide (NO), and endothelium-derived hyperpolarizing factor (EDHF) (6, 9, 26). Endothelial dysfunction is thus characterized by a reduction in the activity of PGI_2, NO, and EDHF, thereby enhancing vasoconstrictor responses mediated by endothelin, serotonin, and thrombin (26). Endothelial injury secondary to myocardial ischemia-reperfusion (I/R) decreases the production and activity of EDRFs in acute myocardial infarction (18).

Among the three different EDRFs, the roles of PGI_2 and NO have been extensively investigated (6, 9, 26). Regarding EDHF, since the first reports on its existence (6, 9), several candidates for EDHF have been proposed, including cytochrome *P*-450 metabolites (2, 4), endothelium-derived K^+ (7), and electrical communications through gap junctions between endothelial cells and vascular smooth muscle cells (29). Matoba et al. (16, 17) have previously identified that endothelium-derived H_2O_2 is a primary EDHF in mesenteric arteries of mice and humans. Morikawa et al. (21) have recently confirmed that endothelial Cu,Zn-SOD plays an important role as an EDHF synthase in mice. We have subsequently confirmed the importance of H_2O_2 in canine coronary microcirculation during coronary autoregulation with reduced coronary perfusion pressure in vivo (35).

However, it remains to be examined whether H_2O_2 also exerts cardioprotective effects during I/R in the coronary microcirculation in vivo, and if so, whether such effects of H_2O_2 compensate the impaired NO-mediated responses due to I/R injury in vivo. In this study, we tested our hypothesis that H_2O_2 plays an important cardioprotective and compensatory role during coronary I/R injury in dogs in vivo.

METHODS

This study conformed to the Guideline on Animal Experiments of Kawasaki Medical School, and approved by an independent review committee from the same institution, and the *Guide for the Care and Use of Laboratory Animals* published by the National Institutes of Health.

Animal preparation. Anesthetized mongrel dogs (15–25 kg in body wt, n = 50) of either sex were ventilated with a ventilator (model VS600, IDC, Pittsburgh, PA). Aortic pressure and left ventricular (LV) pressure were continuously monitored with a catheter (SPC-784A, Millar, TX). The blood flow of the left anterior descending coronary artery (LAD) was continuously measured by a transonic flow probe (T206, Transonic Systems, Ithaca, NY).

Address for reprint requests and other correspondence: T. Yada, Dept. of Medical Engineering and Systems Cardiology, Kawasaki Medical School, 577 Matsushima, Kurashiki, Okayama 701-0192, Japan (e-mail: yada@me.kawasaki-m.ac.jp).

The costs of publication of this article were defrayed in part by the payment of page charges. The article must therefore be hereby marked "*advertisement*" in accordance with 18 U.S.C. Section 1734 solely to indicate this fact.

Measurements of coronary diameter by intravital microscope. We continuously monitored coronary vascular responses by an intravital microscope (VMS 1210, Nihon-Kohden, Tokyo) with a needle probe in vivo as previously described (32). We gently placed the needle probe on subepicardial microvessels. When a clear vascular image was obtained, end-diastolic vascular images were taken with 30 pictures/s (32).

Measurements of regional myocardial blood flow. Regional myocardial blood flow was measured by the nonradioactive microsphere (Sekisui Plastic, Tokyo) technique, as previously described (20). Briefly, the microsphere suspension was injected into the left atrium 85 min after the onset of coronary occlusion. Myocardial collateral flow in the apex during suturing of the collateral vessels from the left circumflex artery (LCX) was calculated according to the formula: time flow = tissue counts × (reference flow/reference counts) and was expressed in milliliters per gram per minute (20).

Detection of H_2O_2 and NO production. 2′,7′-Dichlorodihydrofluorescein diacetate (DCF, Molecular Probes, Eugene, OR) and diaminorhodamine-4M AM (DAR, Daiichi Pure Chemicals, Tokyo) were used to detect H_2O_2 and NO production in coronary microvessels without a different NO scavenger (e.g., methylene blue), respectively, as previously described (21). Briefly, fresh and unfixed heart tissue was cut into several blocks and frozen in optimal cutting temperature compound (Tissue-Tek, Sakura Fine Chemical, Tokyo) within a few hours. Fluorescent images of [illegible] after application of ACh by using [illegible] pus BX51, Tokyo) (21). We used different animals for the [illegible] treatment (DCF and DAR) and the 2,3,5-triphenyltetrazolium chloride (TTC) treatment.

Western blotting. Portions of myocardial samples were homogenized in lysis buffer. After centrifugation, the supernatants were used for Western immunoblotting. The proteins were transferred by semi-dry electroblotting to polyvinylidene difluoride membranes. The blots were then blocked and incubated with horseradish peroxidase-conjugated rabbit anti-endothelial NO synthase (eNOS, dimer form) polyclonal antibody (Santa Cruz Biotechnology, Santa Cruz, CA) or anti-actin antibody (Santa Cruz Biotechnology). The antibody was visualized by using an enhanced chemiluminescence method (ECL; Amersham Biosciences, Tokyo). The integrated density of the bands was quantified by using NIH Image analysis, and the protein expression level of eNOS was normalized to that of actin (24).

Experimental protocols. After the surgical procedure and instrumentation, at least 30 min was allowed for stabilization while hemodynamic variables were monitored. The following protocols were examined.

Coronary vascular responses to endothelium-dependent [ACh, 0.5 and 1.0 μg/kg intracoronary (ic)] and -independent [sodium nitroprusside (SNP), 40 and 80 μg/min ic] vasodilators were examined before ischemia (90 min)-reperfusion (60 min) (I/R). ACh and SNP were continuously and retrogradely infused into the diagonal branch of the LAD by using a syringe pump (STC 525, Terumo, Tokyo). The coronary vascular responses to ACh and SNP were examined for 2 min, and the image of maximal vasodilatation was taken at 2 min of infusion of ACh or SNP.

Coronary vasodilator responses to ACh and SNP were examined before and after coronary ischemia (90 min)-reperfusion (60 min) by proximal LAD occlusion under the following seven conditions with cyclooxygenase blockade (ibuprofen, 12.5 mg/kg iv) to evaluate the [illegible] and NO without PGI$_2$ in a different set of animals (Fig. [illegible]-arginine (L-NMMA) [illegible] and 240,000 U·kg [illegible] H_2O_2 into water and oxygen), *4*) adenosine receptor blockade alone [8-sulfophenyltheophylline (8-SPT), 25 μg·kg^{-1}·min^{-1} ic for 5 min], *5*) catalase plus L-NMMA, *6*) catalase plus tetraethylammonium [TEA, 10 μg·kg^{-1}·min^{-1} ic for 10 min, an inhibitor of large-

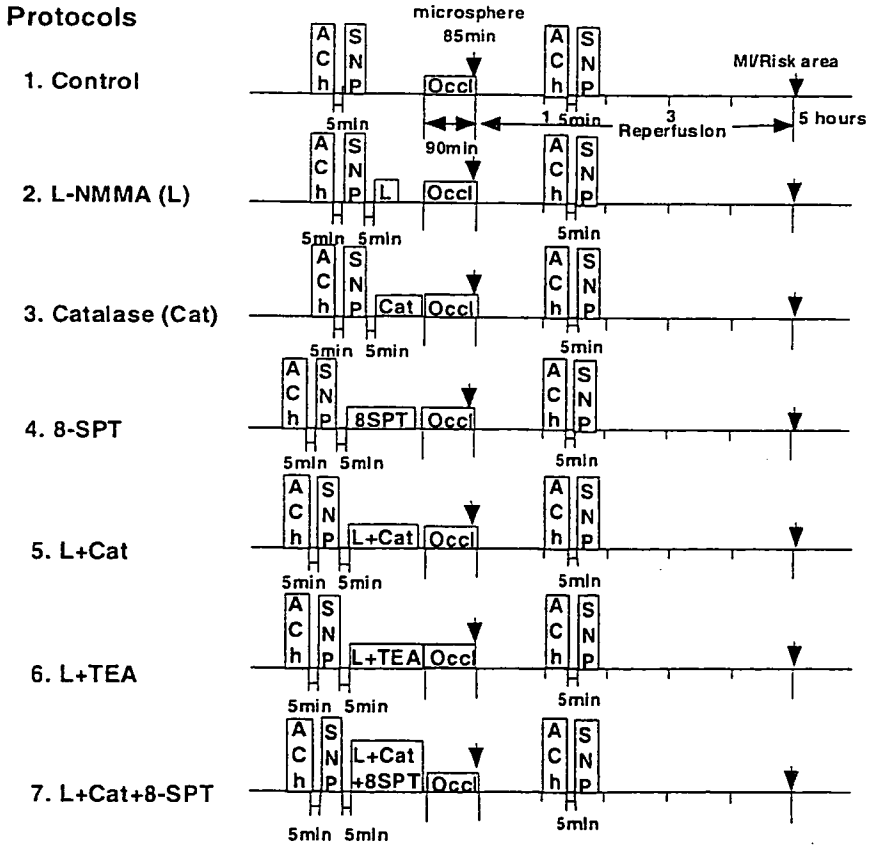

Fig. 1. Experimental protocols. TEA, tetraethylammonium; 8-SPT, 8-sulfophenyltheophylline; ACh, acetylcholine; SNP, sodium nitroprusside; Occl, coronary occlusion; Cat, catalase; L-NMMA (L), N^G-monomethyl-L-arginine; MI, myocardial infarction.

Table 1. *Hemodynamics during coronary ischemia-reperfusion injury in dogs*

		Before I/R			Ischemia (85 min)	After I/R		
	n	Baseline	ACh	SNP		Baseline	ACh	SNP
MBP, mmHg								
Control	5	92±4	91±6	92±5	93±14	92±4	91±5	92±6
L-NMMA	5	97±8	98±7	94±9	92±10	97±7	98±8	95±8
Cat	5	96±8	92±8	94±9	92±9	96±7	96±8	98±6
L-NMMA + Cat	5	94±4	93±9	97±9	95±11	95±8	98±5	94±5
L-NMMA + TEA	5	95±12	93±13	95±14	94±10	91±14	93±15	98±10
L-NMMA + Cat + 8-SPT	5	95±3	96±4	95±3	93±11	96±3	97±4	95±3
Heart rate, beats/min								
Control	5	152±5	155±3	154±3	156±7	156±5	154±5	153±5
L-NMMA	5	157±5	156±5	157±6	158±6	153±5	153±5	153±5
Cat	5	155±4	159±6	158±5	157±6	151±7	155±8	154±8
L-NMMA + Cat	5	156±12	158±13	158±13	154±5	156±13	156±14	159±13
L-NMMA + TEA	5	153±13	154±12	155±11	155±5	150±10	151±11	152±10
L-NMMA + Cat + 8-SPT	5	152±7	155±9	153±3	153±5	152±7	151±6	153±7

Results are expressed as means ± SE; *n* = no. of dogs. I/R, ischemia-reperfusion; MBP, mean blood pressure; Cat, catalase; SNP, sodium nitroprusside; TEA, tetraethylammonium; 8-SPT, sulfophenyltheophylline; L-NMMA, N^G-monomethyl-L-arginine.

conductance Ca^{2+}-sensitive potassium (K_{Ca}) channels], and *7*) catalase plus L-NMMA with 8-SPT (35). These inhibitors were given at 30 min before I/R. An interval between each treatment was 5 min. The basal coronary diameter was defined as that before administration of ACh or SNP either before or after I/R. L-NMMA, catalase, TEA, and 8-SPT were administered alone at 5 min after administration of ACh or SNP. Microspheres were administered at 85 min after the initiation of coronary occlusion. In the combined infusion (L-NMMA + catalase + 8-SPT), catalase solution was infused into the LAD at a rate of 0.5 ml/min at 5 min after infusion of L-NMMA, and then 8-SPT was added into the LAD at 15 min after the initiation of L-NMMA.

After 1 h of reperfusion, coronary vasodilator responses to ACh and SNP were examined.

After 5 h of reperfusion, we reoccluded the LAD and injected Evans blue dye into a systemic vein. Then, myocardial slices (5 μm thick) were incubated in 1% TTC (Sigma) solution to detect the infarct area (36). Different animals were used for fluorescent treatment (DCF and DAR) and TTC treatment.

Drugs. All drugs were obtained from Sigma Chemical and were diluted in a physiological saline immediately before use.

Statistical analysis. Results are expressed as means ± SE. Vascular responses (see Figs. 3*C*, 5*F*, 6*F*, 7, and 9*A*) were analyzed by one-way ANOVA followed by Scheffé's post hoc test for multiple comparisons. Difference in the effects of ACh and SNP on subepicardial coronary microvessels before and after I/R (see Figs. 3, *A* and *B*, 4, and 8, *A* and *B*), and difference between infarct size/risk area and transmural collateral flow in control and other inhibitors (see Fig. 9*B*) were examined by a multiple regression analysis by using a model in which the change in coronary diameter was set as a dependent variable (y) and vascular size as an explanatory variable (x), while the statuses of control and other inhibitors were set as dummy variables (D_1, D_2) in the following equation: $y = a_0 + a_1x + a_2D_1 + a_3D_2$, where a_0 through a_3 are partial regression coefficients (36). The criterion for statistical significance was at $P < 0.05$.

RESULTS

Hemodynamics and blood gases during I/R injury. Immediately after reperfusion, coronary blood flow was increased and some arrhythmias occurred; however, those changes returned to the control levels 1 h after reperfusion when we repeated the measurements. Thus, throughout the experiments, mean aortic pressure and heart rate at baseline were constant and comparable, and Po_2, Pco_2, and pH were maintained within the physiological ranges (pH 7.35–7.45, Po_2 > 70 mmHg, and Pco_2 25–40 mmHg,). Hemodynamic variables at baseline did not significantly change after I/R compared with those before I/R (Tables 1 and 2).

Dose responses to ACh and SNP. ACh (0.5 and 1.0 μg/kg ic) and SNP (40 and 80 μg/min ic) caused coronary vasodilatation in a dose-dependent manner at both small arteries and arterioles (Fig. 2). Then we chose the maximal dose of the vasodilators (ACh, 1.0 μg/kg ic, and SNP, 80 μg/min ic) in the following experiments.

Endothelium-dependent coronary vasodilatation before and after I/R. There was no significant difference in baseline diameter after ACh before I/R among the groups. All inhibitors did not affect resting coronary artery diameter or coronary

Table 2. *Baseline vascular diameter before I/R in response to ACh*

	Small Artery	Arteriole
Control	104–150 μm (120±7, *n* = 7)	37–96 μm (70±6, *n* = 12)
L-NMMA	106–164 μm (131±7, *n* = 8)	36–95 μm (63±5, *n* = 16)
Cat	100–147 μm (121±5, *n* = 10)	28–89 μm (61±6, *n* = 12)
8-SPT	114–162 μm (130±8, *n* = 6)	30–88 μm (60±10, *n* = 5)
L-NMMA + Cat	102–141 μm (118±5, *n* = 8)	34–95 μm (77±4, *n* = 10)
L-NMMA + TEA	105–142 μm (123±6, *n* = 5)	34–95 μm (62±9, *n* = 8)
L-NMMA + Cat + 8-SPT	110–145 μm (128±6, *n* = 5)	38–87 μm (67±7, *n* = 7)

Results are expressed as range (means ± SE); *n* = no. of blood vessels.

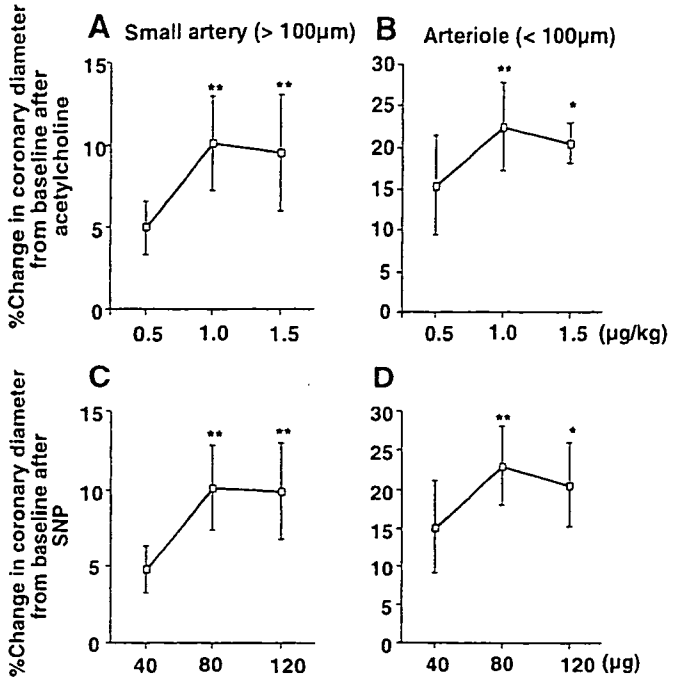

Fig. 2. Dose responses to ACh (*A* and *B*) and SNP (*C* and *D*) before ischemia-reperfusion (I/R). Number of small arteries (*A* and *C*) and arterioles (*B* and *D*) per animals used was 5/5 for each group. $*P < 0.05$, $**P < 0.01$ vs. ACh (0.5 μg/kg) and SNP (40 μg).

blood flow. Under control conditions (before I/R), intracoronary administration of ACh caused a significantly greater coronary vasodilatation in arterioles than in small arteries (Fig. 3, *A* and *B*). Coronary I/R significantly impaired the coronary vasodilatation to ACh in both sized arteries (Figs. 3*A* and 4*A*), and L-NMMA reduced the vasodilatation in small arteries (Figs. 3*A* and 4*B*) but rather increased the response in arterioles compared with control (Figs. 3*B* and 4*A*) after I/R. Catalase and 8-SPT increased the ACh-induced vasodilatation in small arteries (Figs. 3*A* and 4, *C* and *D*) but decreased the response in arterioles (Fig. 3*B*) after I/R. There was no significant difference in coronary blood flow before and after I/R among the control, the L-NMMA, and the catalase group (Fig. 3*C*). L-NMMA + catalase (Figs. 3, *A* and *B*, and 4*E*) or L-NMMA + TEA (Figs. 3, *A* and *B*, and 4*F*) decreased the vasodilatation in both sized arteries (Fig. 3, *A* and *B*) with decrement of coronary blood flow (Fig. 3*C*), and L-NMMA plus catalase with 8-SPT further decreased the vasodilatation in both sized arteries (Figs. 3, *A* and *B*, and 4*G*) compared with other groups (Fig. 3, *A–C*).

Detection of H_2O_2 and NO production. Fluorescent microscopy with DCF showed that I/R increased the vascular H_2O_2 production in control LCX (Fig. 5, *B* and *F*) compared with baseline conditions (Fig. 5, *A* and *F*) and decreased the H_2O_2 production in control LAD (Figs. 5, *C* and *F*), which was enhanced by L-NMMA (Fig. 5, *D* and *F*) and was abolished by catalase (Fig. 5, *E* and *F*) in arterioles. By contrast, the production of NO as assessed with DAR fluorescence was increased in control LCX (Fig. 6, *B* and *F*) compared with baseline LCX (Fig. 6, *A* and *F*) after I/R, decreased in control LAD (Fig. 6, *C* and *F*), inhibited by L-NMMA (Fig. 6, *D* and *F*), and was enhanced by catalase (Fig. 6, *E* and *F*) in small arteries.

Western blotting of eNOS protein expression in myocardium. In the control group, expression of eNOS protein in the ischemic LAD area was significantly decreased compared with the nonischemic LCX area (Fig. 7). In the catalase group, this decrease in the eNOS protein expression was inhibited by catalase (Fig. 7).

Endothelium-independent coronary vasodilatation. Coronary vasodilator responses to SNP were comparable under all conditions in both sized arteries (Fig. 8). Those coronary vasodilator responses were resistant to the blockade of NO synthesis with L-NMMA (Fig. 8).

Effect of H_2O_2 on I/R-induced myocardial infarct size. I/R injury caused myocardial infarction, the size of which was ~40% of the LV risk area (Fig. 9*A*). Intracoronary L-NMMA, catalase, or 8-SPT alone did not further increase the I/R-induced infarct size (Fig. 9*A*). By contrast, intracoronary L-NMMA plus catalase or TEA markedly increased the infarct size, and L-NMMA plus catalase with 8-SPT further increased

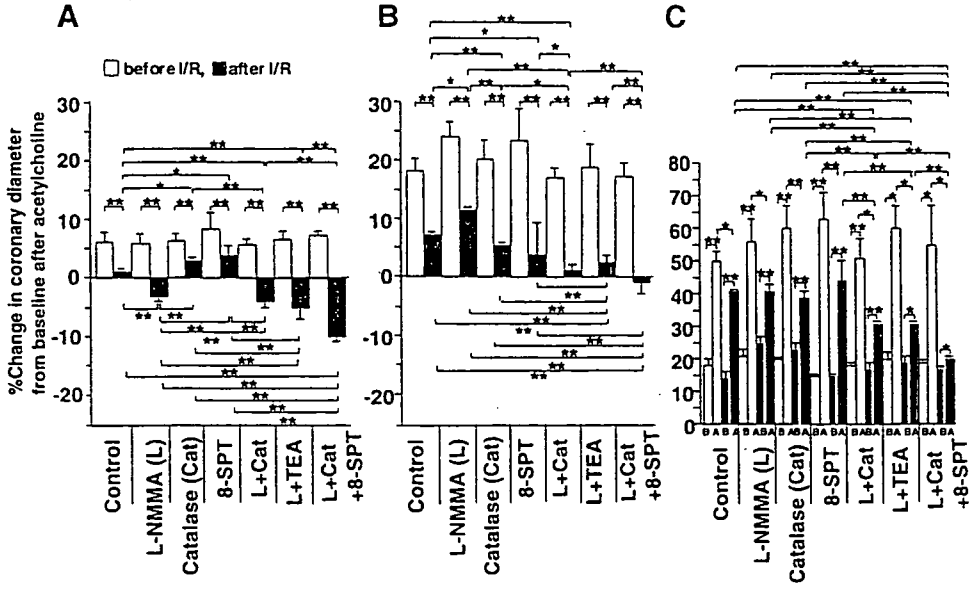

Fig. 3. Endothelium-dependent coronary vasodilatation to ACh before and after coronary I/R injury in dogs in vivo. *A*: small artery (≥100 μm). *B*: arteriole (<100 μm). *C*: coronary blood flow (CBF). No. of small arteries or arterioles per animals (*n/n*) used was 7/5 for control, 8/5 for L-NMMA, 10/5 for catalase, 6/5 for 8-SPT, 8/5 for L-NMMA plus catalase, 5/5 for L-NMMA plus TEA, and 5/5 for L-NMMA plus catalase plus 8-SPT in small arteries; and 12/5 for control, 16/5 for L-NMMA, 12/5 for catalase, 5/5 for 8-SPT, 10/5 for L-NMMA plus catalase, 8/5 for L-NMMA plus TEA, and 7/5 for L-NMMA plus catalase plus 8-SPT in arterioles. No. of animals during the measuring CBF used was 5 for each group. B, before ACh; A, after ACh. $*P < 0.05$, $**P < 0.01$.

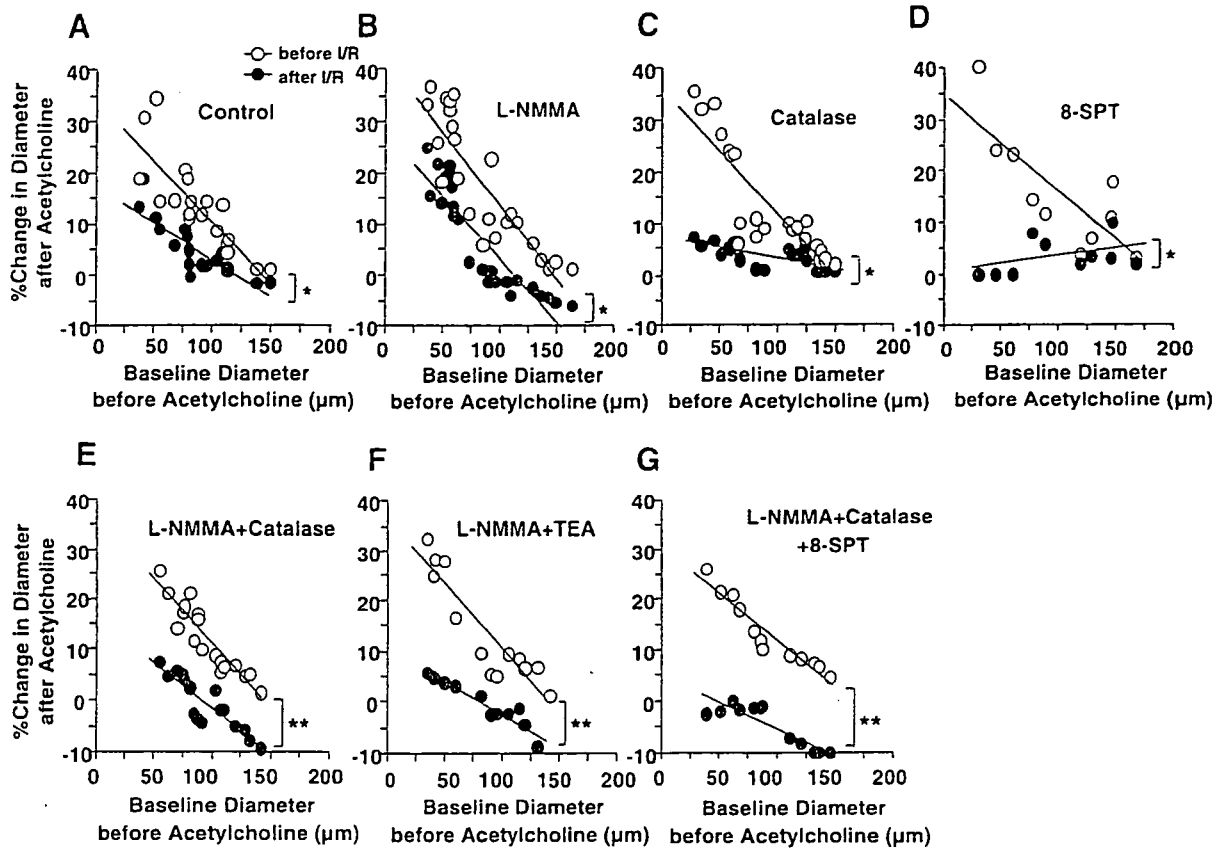

Fig. 4. Percent change in diameter after ACh before and after coronary I/R injury in dogs in vivo. No. of small arteries and arterioles per animals used was 7/5 for control (*A*), 8/5 for L-NMMA (*B*), 10/5 for catalase (*C*), 6/5 for 8-SPT (*D*), 8/5 for L-NMMA plus catalase (*E*), 5/5 for L-NMMA plus TEA (*F*), and 5/5 for L-NMMA plus catalase plus 8-SPT in small arteries (*G*); and 12/5 for control (*A*), 16/5 for L-NMMA (*B*), 12/5 for catalase (*C*), 5/5 for 8-SPT (*D*), 10/5 for L-NMMA plus catalase (*E*), 8/5 for L-NMMA plus TEA (*F*), and 7/5 for L-NMMA plus catalase plus 8-SPT in arterioles (*G*). $^*P < 0.05$, $^{**}P < 0.01$.

the infarct size (Fig. 9*A*). In the control group, there was an inverse relation between the infarct size and transmural collateral blood flow measured by microsphere technique ($r = 0.90$, $P < 0.01$). There was no significant difference in the relationship among the control, L-NMMA, and catalase treatment (Fig. 9*B*). L-NMMA plus catalase or TEA significantly shifted the regression line upward compared with the control group (both $P < 0.01$), and L-NMMA plus catalase with 8-SPT further shifted the regression line upward compared with L-NMMA plus catalase or TEA (Fig. 9*B*, both $P < 0.01$).

DISCUSSION

The major finding of the present study is that endogenous H_2O_2, in cooperation with NO, plays an important cardioprotective role during coronary I/R injury as a compensatory mechanism for NO in vivo. To the best of our knowledge, this is the first report that demonstrates the important protective role of endogenous H_2O_2, in cooperation with NO, against coronary I/R injury in vivo.

Validations of experimental model and methodology. On the basis of the previous reports (22, 31), we chose the adequate dose of ACh, SNP, L-NMMA, catalase, TEA, and 8-SPT to examine the effects of endothelium-dependent and -independent coronary vasodilator responses and inhibition of NO synthesis, H_2O_2, K_{Ca} channels, and adenosine receptor, respectively. In addition, on the basis of previous studies and our own (31, 35), we choose the doses of ACh and SNP that cause maximal coronary vasodilatation in dogs in vivo. TEA at low doses is fairly specific for K_{Ca} channel, but at higher doses it may block a number of other K channels. Because several K_{Ca} channels are involved in H_2O_2-mediated responses (26), we selected the nonselective K_{Ca} inhibitor TEA to inhibit all K_{Ca} channels (15). We have previously confirmed the validity of the methods that we used in the present study (32). After 60–90 min of ischemia, ultrastructural damage of coronary endothelium was observed particularly in the subendocardium in the present study, a finding consistent with the previous study (8).

H_2O_2 during coronary I/R in vivo. It was previously reported that relaxations of isolated large canine coronary arteries to exogenous H_2O_2 were partially endothelium dependent (23). Recently, Matoba et al. (16, 17) identified that endothelium-derived H_2O_2 is an EDHF in mouse and human mesenteric microvessels. Subsequently, we (35) and others (19) have confirmed that endogenous H_2O_2 exerts important vasodilator effects in canine coronary microcirculation in vivo and in isolated human coronary microvessels, respectively. It is conceivable that H_2O_2 is produced from superoxide anions derived from several sources in endothelial cells, including eNOS, cyclooxygenase, lipoxygenase, cytochrome *P*-450 enzymes, and NAD(P)H oxidases (16). In the present study, L-NMMA or catalase alone did not com-